Deep–Sea Research II 180 (2020) 104845

Contents lists available at ScienceDirect

Deep-Sea Research Part II

journal homepage: http://www.elsevier.com/locate/dsr2

# Fine-scale observations of physical and biological environment along a herring feeding migration route

Webjørn Melle [a,*], Thor Klevjer [a], Espen Strand [a], Peter H. Wiebe [b], Aril Slotte [a], Geir Huse [a]

[a] Institute of Marine Research, Bergen, Norway
[b] Woods Hole Oceanographic Institution, USA

ARTICLE INFO

*Keywords:*
Herring
Feeding migration
Environment
Prey distribution
Fine-scale observation

ABSTRACT

We observed herring horizontal and vertical distribution during feeding migration along a 128 km transect across the Arctic front of the Norwegian and Iceland seas, in early June, in relation to its physical, chemical and biological environment, distribution of prey organisms and pelagic and mesopelagic competitors. The Norwegian Spring Spawning herring is one of the largest and economically most important stocks of pelagic fish in the world and understanding what controls its feeding migration is, and has been for centuries, a major research question that also has major implications for management. High resolution ecosystem data were obtained by hull mounted multi-frequency acoustics and a towed platform undulating between 10 and 400 m equipped with multi-frequency acoustics, temperature, salinity and fluorescence sensors, an Optical Plankton Counter and a Video Plankton Recorder. Additional sampling was done by MOCNESS, Macroplankton trawl, and CTD equipped with water bottles for temperature, salinity, nutrients and chlorophyll at discrete stations along the transect. Biological characteristics and stomach content of the herring were obtained from samples at discrete trawl stations. The Arctic front proved to be an important transitional zone in zooplankton biomass, abundance and diversity. Phenology of phyto- and zooplankton also changed across the front, being somewhat delayed on the cold side. The herring were distributed all along the transect showing a shallow distribution on the warm side and both deep and shallow on the cold side, not clearly related to light and time of the day. The herring stomach content was higher on the cold side. There was no significant pattern in average age, weight, or body length of the herring along the transect. The herring were present and fed in the area of the transect during the time when the overwintering generation of *Calanus finmarchicus* dominated, before the development of the new generation of the year. We suggest that the phenology of *C. finmarchicus* can be an important driver of the herring feeding migration. While prey-availability was higher on the Arctic side of the front, light conditions for visual feeding at depth were probably better on the Atlantic side. The herring did not show classical dial vertical migration, but its prey did, and the herring's prey were probably available within the upper 100 m during the course of a 24 h cycle. With a general westward direction of migration, the herring along the transect moved towards lower temperatures and temperature did not seem to be a probable driver for migration. We conclude that fine-scale studies of herring migration and feeding can increase our understanding of the migratory processes and add to our understanding of large-scale distributional patterns, changes therein, and herring trophodynamics and ecological role. The fine-resolution parameters can also be important as input to ecosystem models.

## 1. Introduction

The migration pattern of the Norwegian Spring Spawning Herring has fascinated oceanographers as well as fishers and inhabitants of the North Atlantic coastal communities for centuries (Dragesund, 1970; Dragesund et al., 1997; McQuinn, 1997; Misund et al., 1997, 1998; Fernö et al., 1998; Jakobsson and Østvedt, 1999; Corten, 2002; Holst et al., 2002; Huse et al., 2010). Not only the basin wide nature of the migration, but also the large and often abrupt geographical variability bringing prosperity or ruin to numerous places along the northern European coasts and forcing the oceanic fishing fleet to search for herring ever further from their home ports.

The Norwegian and Iceland Seas ecosystem, the home of the herring, is characterised by a northward flowing warm Atlantic current in the

* Corresponding author. Institute of Marine Research, P.O box 1870 Nordnes, NO-5817, Bergen, Norway.
*E-mail address:* webjoern.melle@hi.no (W. Melle).

https://doi.org/10.1016/j.dsr2.2020.104845
Received 22 December 2019; Received in revised form 4 June 2020; Accepted 2 August 2020
Available online 19 August 2020

east, while in the west cold Arctic water generally flows towards the south and east (Blindheim, 2004). The water masses represent two distinct habitats inhabited by warm and cold-water species like *C. finmarchicus* and the larger *C. hyperboreus*, respectively, and *Calanus* spp. is considered the main food item of the Norwegian spring spawning (NSS) herring (Dalpadado et al., 2000). These ecosystems display a pronounced spatial pattern in phyto- and zooplankton phenology. Along a southeast-northwest axis, the formation of the seasonal thermocline, the start and development of the phytoplankton spring bloom, and the ontogenetic migration and reproduction and development of *Calanus* spp. tend to start in the southeast and progress towards the northwest (Fernö et al., 1998; Melle et al., 2004; Broms et al., 2007, 2009, 2012; Bagøien et al., 2012; Erga et al., 2014; Dupont et al., 2017). This pattern has also been observed across the Arctic front and between water masses.

The NSS herring stock spawn along the Norwegian coast in April (Runnstrøm, 1941; Nøttestad et al., 1996) and thereafter migrate westward, soon after occurring just east of the Arctic front (Misund et al., 1997; Nøttestad et al., 2007; Fernö et al., 1998). This westward feeding migration is an important feature of the annual cycle of the NSS herring and spreads the stock out over the Norwegian and Iceland Seas ecosystem. Looking at interannual relationships between herring stock size and zooplankton biomass, studies have indicated that there is a top down large-scale effect by herring on its zooplankton prey in the Norwegian Sea (Olsen et al., 2007; Huse et al., 2012). Towards the end of the feeding migration, in July, sonar studies have revealed that herring schools can migrate in various directions both towards and away from their overwintering area located west of Northern Norway, at the time (Kvamme et al., 2003).

While the ultimate reason for the predominantly westward migration is feeding, we have a limited understanding of the proximate cues and drivers of the feeding migration. In practice the westward feeding migration takes the herring into ever colder water, but Broms et al. (2012) concluded that prey density was the major driver of the westward migration. Prey densities were related to spatial (across oceanic fronts) and temporal (within water masses) patterns in phenology of its major prey, *Calanus finmarchicus*, so that herring densities peaked where number of copepodite stage V and adults of the ascending overwintering generation of *C. finmarchicus* peaked in the surface waters.

The interpretation of herring behaviour is complicated by apparent elements of learned, social behaviour, in addition to "evolved" behaviour (Fernö et al., 1998). The overarching rationale is that environmental changes in the Norwegian and Icelandic seas, and the response of the prey of herring to these changes, make it hard to predict if and how herring migrations may change in the future. A more mechanistic understanding of drivers of herring migration may enable such predictions.

In order to get a better understanding of these drivers, we measured biological and physical gradients along the herring migrations at finer scales. The focus was on the part of the feeding migration when the herring crosses the Arctic front in the western Norwegian Sea into the Icelandic Sea during early summer (Nøttestad et al., 2007; Utne et al., 2012). By focusing on a relatively short segment along the perceived migration route and the leading schools of the herring, while applying new underwater observation technology, enabling very fine-scale resolution of physical and biological parameters, we aimed at disclosing the relationship between the herring distribution and temperature and prey density, and whether the latter could be explained by spatial patterns in prey phenology or differences in species diversity between Atlantic and Arctic water masses.

## 2. Material and methods

### 2.1. Observational design

During the Norwegian Euro-BASIN cruise from Bergen (Norway) to Nuuk (Greenland) and the return to Bergen (1 May – 14 June 2013), a period of 3 days (7–10 June) was devoted to the study of the migration and feeding behaviour of the herring near the Arctic front, between Jan Mayen and Iceland in the western Norwegian Sea (Fig. 1). After locating the Arctic front, and mapping the wider area acoustically to locate the herring, a transect across the front was mapped on a fine vertical and horizontal scale, while towing a combined optical and acoustic platform, MESSOR (see details below), undulating between 10 and 400 m. After that the transect was sampled with respect to herring and macrozooplankton using trawls, mesozooplankton with nets, and hydrography, chlorophyll, and nutrients with a CTD carrying 12 water bottles.

### 2.2. Hydrography, nutrients and chlorophyll

Hydrography and fluorescence were sampled with MESSOR (see description below) along the MESSOR transect (Table 1, Fig. 1). Additional CTD casts were taken in connection with all trawl and net stations, to a depth of 500 m. From the water bottles on the CTD, samples for chlorophyll and nutrients were collected and analysed according to Bagøien et al. (2012). The chlorophyll and nutrient measurement used in the present analysis were from the upper 100 and 200 m, respectively. Underway continuous measurements of temperature, salinity and fluorescence were obtained from a water intake at 8.5 m depth.

### 2.3. Herring, micro-nekton and zooplankton net sampling and onboard and laboratory analyses

The herring were sampled by 6 pelagic trawl hauls (Multpelt – ICES, 2013), aiming at schools observed with the acoustic equipment at daytime, or surface hauls at night using large floats on the trawl wingtips (Table 1, Fig. 1). The catch was sorted on deck and all species were identified and weighed. A subsample of at least 100 herring was used to measure total length (cm) and individual total weight (g). From at least 30 herring, stomachs were extracted, preserved frozen and analysed in the lab on land to get the individual diet of the herring. The food items were identified to species and life stage when possible or to broader taxonomic groups.

The meso-zooplankton were sampled by 4 oblique hauls with a 1-$m^2$ MOCNESS (Wiebe et al., 1985), equipped with 180 μm nets, from 400 to 0 m (Table 1, Fig. 1). The 8 nets sampled the depth horizons 400 – 300 m, 300 – 250 m, 250 – 200 m, 200 – 150 m, 150 – 100 m, 100 – 50 m, 50 -25 m, 25 – 0 m. Two MOCNESS stations were in Atlantic water, one was at the front, and one was in Arctic water.

The zooplankton samples were treated on deck as described by Melle et al. (2004), resulting in one half of the sample divided into three size fractions (<180, 1000–2000, and >2000 μm) that were dried and weighed, while the other half was fixed in formalin and subsequently identified and counted under the microscope. The MOCNESS effectively catches meso-zooplankton, while macrozooplankton have the capacity to avoid and the micro-zooplankton are extruded through the meshes. The smaller organisms like eggs, nauplii, and copepodite stages I to III were excluded from the total abundance data before analyses started, except for the analysis of *Calanus finmarchicus* developmental stage distribution. The reason for this was to reduce the total dominance of these smaller taxa that is not considered to be prey of adult herring (Dalpadado et al., 2000), in the subsequent analyses. Further, we will not present results for taxa that were not identified as herring prey at the species level or higher, since we think this will go beyond the objective of the present article as well as obscuring the results as the number of taxa is high.

To catch larger species of plankton and smaller nekton present, we used a Macroplankton trawl twice, between 0 and 400 m. One haul was placed in Arctic and one in Atlantic water. This trawl was hauled obliquely between 0 and 400 m and back to 0 m at about 2.2 knots. The Macroplankton trawl has a 36 $m^2$ mouth opening and 3 × 3 mm squared meshes or light opening along the entire net (Melle et al., 2006; Wenneck et al., 2008; Krafft et al., 2010; Heino et al., 2011). All samples

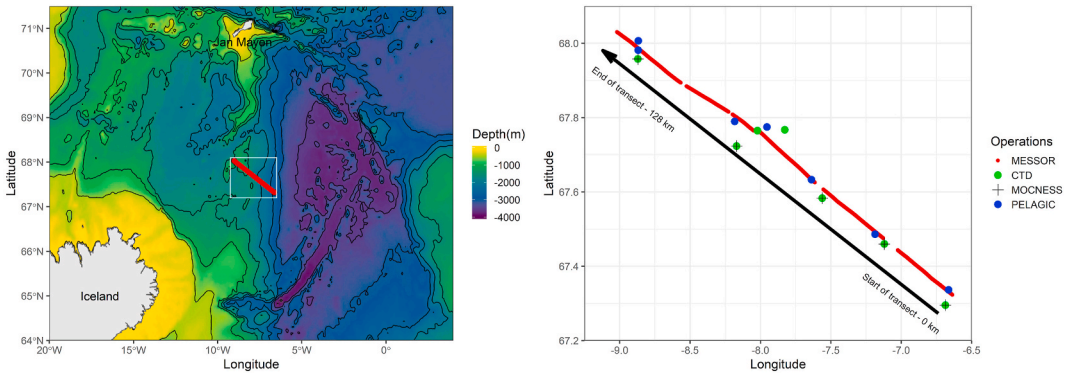


**Fig. 1.** Map of investigation area in the north-western Norwegian Sea with position of the transect across the Arctic front (MESSOR tows) and the location of CTDs, trawls and plankton nets. Two Macroplankton trawls in Atlantic (63.8$^0$ N, 2.3$^0$ E) and Arctic (68.4$^0$ N, 10.4$^0$ W) water masses located outside the range of the transect, are not shown.

**Table 1**
Sampling of hydrography, nutrients, chlorophyll, plankton, micronekton and herring by Multpelt trawl, MOCNESS, Macroplankton trawl, CTD, and MESSOR.

| Equipment | Depth (m) | Comments | No. of stations |
|---|---|---|---|
| MOCNESS | 0–400 | Oblique tow at about 1.8 knots | 4 |
| Multpelt | Upper 400 | Aimed trawling or at surface with floats, about 3 knots | 6 |
| Macroplankton trawl | 0–400 | V-hauls (double oblique), ~2.2 knots | 2 |
| CTD with water bottles | 500 m | Vertical casts | 7 |
| MESSOR | 10–400 | Tow-yoing at 4.5 knots | 1 |

were sorted and identified to taxonomic groups (species or coarser taxonomic groups) on board. For each group biomass and abundance were determined, and length and individual weight of all or at least 100 specimens were recorded. Organisms like krill, amphipods and large copepods that are caught in the trawl are common food items in herring stomachs (Gislason and Astthorsson, 2002; Bachiller et al., 2016).

### 2.4. Acoustic observations by hull-mounted transducers

Acoustic data from the ships echosounders, Simrad EK60 with 18, 38, 70, 120, 200, and 333 kHz transducers mounted on a drop-keel at 6 m depth, were collected and analysed using the standard IMR protocol (ICES, 1982, 2008), using LSSS (Large Scale Survey System) with KORONA (Korneliussen et al., 2006, 2016) to describe the horizontal and vertical distribution and density of herring. The echosounders on the vessel were calibrated using the standard sphere method (Demer et al., 2015) prior to the cruise.

In order to estimate area biomass density of herring we used acoustic data from the hull mounted 38 kHz transducer and catch measurements. The average length of herring (~35.5 cm) were used to estimate the average herring TS, using the standard TS to length equation (TS = 20logL – 71.9, Foote, 1987). Using the average TS, the per segment NASC values were then converted to numerical densities of herring along the transect, which were converted to biomass densities using the average herring weight from the catches (~315 g). The average biomass density for the whole area was taken as the simple average of these per segment biomasses.

### 2.5. Fine-scale mapping with MESSOR

In between net and CTD sampling, we used a towed platform MESSOR (Knutsen et al., 2013) to map the transect. MESSOR was equipped with multifrequency acoustics (Simrad EK60 with 38, 70, 120, 200 and 333 kHz transducers mounted on the bottom plate of MESSOR), optical imaging (VPR - Davis et al., 1992) and particle counting (OPC - Herman, 1992) systems, fluorometer, temperature, and salinity sensors. The fluorometer was calibrated by comparing with chlorophyll measurements from water bottles at fixed CTD stations along the transect, and compared with a calibrated fluorometer (Naustvoll et al., this issue). The MESSOR echosounders were calibrated according to the standard sphere method (Demer et al., 2015) while the towed body was kept at the surface next to the vessel. This was done in the harbour of Reykjavik, during the cruise. During deployment the echosounders transmitted 512 ms pulses at a rate of ~1 $s^{-1}$.

MESSOR was tow-yoed between 10 and 400 m at a ship speed of ~4.5 knots, while hauling with a wire speed of 0.3 and lowering at a speed of 0.5 m $s^{-1}$. Using data from this platform in combination with hull mounted multi-frequency acoustics provides observations of hydrography, fluorescence, plankton, and fish distributions continuously with a very high resolution along the transect crossing the front.

### 2.6. Post processing of MESSOR acoustic data

Acoustic data from the MESSOR were imported into LSSS and processed in KORONA (Korneliussen et al., 2016). After automatic removal of noise (spike noise and TVG amplified noise), data affected by secondary bottom and surface reflections were manually removed. After cleaning, the data were then integrated at a threshold of -90 dB (at 38, 70, 120, 200, and 333 kHz), in 10 s by 5 m vertical bins as multifrequency Nautical Area Scattering Coefficients (NASC ($m^2$ $nmi^{-2}$) - MacLennan et al., 2002). This bin-data resolution is the base unit for further analysis.

The effective ranges differed for the different frequencies, thus to compare frequency responses and use acoustic results for classification, only data for ranges 20–45 m away from MESSOR were used. In this range all transducers had high signal to noise ratios (SNR >> 10 dB). Due to the lack of depth resolved trawl samples, we have a limited understanding of vertical distribution of the different species in the areas covered by the cruise. We therefore decided to use the multi-frequency acoustics onboard MESSOR to describe vertical patterns of different acoustic categories. Unlike conventional hull-mounted acoustics, the towed platform offers acceptable SNR at depth for the higher frequencies, enabling description of vertical patterns in multifrequency acoustic backscatter spanning the surface to ~ 450 m depth and covering significant parts of the mesopelagic zone in these areas.

In order to avoid too many assumptions about the organisms responsible for the backscatter prior to the analysis, we opted to use simple, empirical descriptors. Data (20–45 m range from MESSOR) were simply grouped according to the frequency of the strongest backscatter. Observation bins where backscattering levels showed signs of

bimodality, e.g. where backscatter did not decrease monotonically with frequency away from the frequency of maximum backscatter, were left as uncategorised. If backscattering peaked at 38 kHz, it was assigned to category 38, if it peaked at 70 kHz, it was assigned to category 70, backscatter peak at 120 kHz was assigned to category 120. If backscatter peaked at either 200 or 333 kHz, it was assigned to the combined category 333. The frequency response of the acoustic categories from the MESSOR data, can to some extent be used to extract information on the taxonomic and size composition of the scatterers. Backscatter peaking at low frequencies is usually interpreted as an indication of presence of air-inclusions. For weakly scattering organisms, e.g. organisms without gas-inclusions, such as crustaceans, expected backscatter is very low when the size of the organisms is much smaller than the wavelength of the echosounder signal. As the frequency increases, the ratio of organism size to wavelength increases, and backscatter is expected to increase. For sampling bins with much higher backscatter at high frequencies compared to the backscatter at low frequencies, we can therefore expect smaller, weakly scattering organisms, such as for instance crustaceans, to be more abundant.

The results of this categorization are presented as echograms. Spatial structure in data recorded during MESSOR deployments were visualized by collapsing all data recorded during a single up- or downcast into a single column with 20 m vertical resolution. In these columns, each vertical "pixel" contains multiple observations (i.e. 5 m vertical "observation" bins classified or "raw" backscatter). Horizontal visualisations ("synthetic echograms", i.e. plots of variable responses in depth and a horizontal dimension (time or distance)) of these spatial data are presented, with each pixel representing the average backscatter per category. Backscattering strength was calculated at the frequency of maximum backscatter, i.e. for the category 38 (peak backscatter at 38 kHz) echogram. The 38 kHz backscatter of all observation bins that were assigned to category 38 has been averaged per depth and cast.

### 2.7. Post processing of MESSOR OPC data

The OPC on MESSOR uses light to detect, size (250 μm to ~2 cm) and count particles that passes through an opening in the instrument (Herman, 1992). The OPC, with a mouth opening of ~50 $cm^2$ was placed at the front of MESSOR, heading forward. The flow through the instrument was taken as the flow outside MESSOR, measured by a flowmeter placed on the top of the vehicle. The volume of water measured was estimated as the product of the mouth opening and the distance travelled. All detected particles are counted and reported at 2 Hz, hence the vertical resolution of the particle size distribution is very high and can be used, for instance, to study vertical patchiness or the presence of vertical aggregations of particles. The major drawback of this sampling gear is the lack of information beyond particle size. The Equivalent Spherical Diameters (ESD) counted and measured by the OPC (as described in Herman, 1992) was subsequently binned according to Basedow et al. (2008), who used size ranges of *Calanus finmarchicus* life stages to bin the ESDs based on laboratory experiments (Table 2). The taxonomic composition of particles counted by the OPC, may, after vertical averaging, be inferred from images obtained by the VPR (see below).

In addition to size classes 3–5 originating from Basedow et al.'s laboratory experiments with *C. finmarchicus* (Table 2), size classes 2 and 6 are also referred to in the Results. Size class 2 were objects with ESDs less than 0.63 mm while ESDs of size class 6 were larger than 2.0 mm. Objects smaller than 250 μm are below the detection range normally used for the OPC (Herman, 1992) and is not shown.

**Table 2**
Size classification of *Calanus finmarchicus* copepodites, used for binning of ESDs (Equivalent Spherical Diameter) of OPC objects (from Basedow et al., 2008).

| Copepodite stage | ESD (mm) | | Size class |
|---|---|---|---|
| | Experiment 1 | Experiment 2 | |
| CII–CIII | 0.63–1.12 | 0.65–1.02 | 3 |
| CIV | 1.12–1.57 | 1.02–1.55 | 4 |
| CV + CVI♀ | 1.57–2.0 | 1.55–2.0 | 5 |

### 2.8. Post processing of MESSOR VPR data

The Video Plankton Recorder (VPR - Davis et al., 1992) continuously takes photographs of particles that passes through the focusing volume. Images are acquired at up to ~ 15 Hz, but each imaged volume is relatively small (45 ml with the settings used). The vertical resolution provided by the VPR is similar to the OPC and having a recorded image of what is present *in situ* is a great advantage. However, compared to the other gear used, the total measured volume per time or per vertical profile is small. In general the quality of the images from the VPR is good enough to sort observations into species groups, but usually not good enough for species identification. The objects observed by the VPR were extracted and analysed using the post-processing program developed and provided by the producer of the VPR (AutoDeck, Seascan Inc - ftp://ftp.library.noaa.gov/noaa_documents.lib/DWH_IR/DWH_documents_NCDDC/Archive%20Prep%202/American_Diver/Cruise_02/0-data/VPR/Documentation/Digital_AutoVPR.pdf) and VisualPlankton (Davis et al., 2004; Hu and Davis, 2006; Gislason et al., 2016). AutoDeck will extract regions of interest (ROI) on every image and save it to file as a vignette. ROIs are regions of an image defined by AutoDeck in accordance with the settings of AutoDeck to be an object (see reference to Seascan Inc for details). The settings of AutoDeck used for the present analysis are given in Table 3. The VPR was calibrated for the magnification setting S2 using CalDeck (Seascan Inc), estimating an observational volume of 45 ml per image (Gislason et al., 2016). AutoDeck added depth from the CTD on MESSOR to each ROI.

With the software Visual Plankton (Hu and Davis, 2006) the ROIs were automatically identified as described by Gislason et al. (2016). Visual Plankton produced a confusion matrix from which we were able to identify 5 groups with high probability according to the statistics of the confusion matrix (Table 4). The selected taxa were the ones with the highest probability of correct prediction in the data set for the whole trans-Atlantic cruise, including the Irminger and Labrador Seas. In the region of the MESSOR transect, we did not have phytoplankton aggregates and this group is not analysed any further (see Strand et al., this issue, for analysis of the phytoplankton aggregates). The four taxa identified in the VPR data and used in the present analysis, were copepods, marine snow, gelatinous plankton, and *Pseudocalanus* females with eggs. The last class is commonly identified in VPR images due to the conspicuous pair of egg sacs attached to their abdomen. These are usually *Pseudocalanus* (Gislason et al., 2016), but *Pareuchaeta* females carry eggs as well and occurred in our nets, though at so low densities that we kept the label "Pseudocalanus" for the VPR category. Visual plankton estimated abundances as individuals $L^{-1}$ based on the sampling volume and number of images.

**Table 3**
Settings of AutoDeck during extraction of ROIs. The effect of the settings is given in the manual of AutoDeck (see above reference to Seascan Inc).

| High Segmentation Threshold | 150 |
|---|---|
| Low Segmentation Threshold | 0 |
| Sobel Threshold | 40 |
| Brightness | 0 |
| Contrast | 100 |
| Focus StdDev | 0 |
| Focus Kernel Size | 3 |
| Minimum Blob Size | 100 |
| Growth Scale | 500 |
| Minimum Join Distance | 1 |

**Table 4**
Confusion matrix of the dual-classification system used to identify objects in the VPR images. See Hu and Davis (2006), and references therein, for details. PD is probability of detection (%) which is based on the ratio of accurate/true automatic classifications to total (manual) identified images belonging in a category. PD is the probability that an image belonging in a class will be classified as a that taxon. SP is specificity (%), which is based on the ratio of automatic classifications actually belonging in a class to total assignments to that class. SP is the probability that the classifier's prediction is correct for each taxon. NA is not applicable. All data are counts, except SP and PD, which are percentages.

| Taxa | Phytopl. aggregates | Copepods | Gelatinous plankton | Marine snow | Pseudocalanus $^{w}$/eggs | Other | SP% |
|---|---|---|---|---|---|---|---|
| Phytopl. aggregates | 193 | 0 | 0 | 1 | 0 | 0 | 99.5 |
| Copepods | 0 | 156 | 6 | 2 | 1 | 4 | 92.3 |
| Gelatinous plankton | 0 | 3 | 112 | 6 | 0 | 12 | 84.2 |
| Marine snow | 0 | 1 | 4 | 120 | 0 | 21 | 82.2 |
| Pseudocalanus $^{w}$/eggs | 0 | 0 | 0 | 0 | 185 | 0 | 100.0 |
| Unknown | 7 | 40 | 78 | 71 | 14 | 144 | 40.7 |
| PD | 97 | 78 | 56 | 60 | 93 | 80 | NA |

### 2.9. Light measurements and the habitat suitability to herring feeding

The combination of net catches and optical and acoustic sensors give us a good overview over densities of potential herring prey present. However, these densities do not necessarily reflect the availability of these prey to the herring. While herring can filter feed they are believed to normally use their vision in the predation process (Batty et al., 1990). We did not have a focus on collecting data on the optical environment during the herring migration study in itself, but we continuously measured surface irradiance every 5 min using a TriOS Ramses hyperspectral irradiance sensor. Over the course of the BASIN cruise, we also collected profiles of underwater irradiances using a similar hyperspectral sensor. We present data from 3 such vertical profiles obtained in the Norwegian and Icelandic Seas. The first vertical profile was obtained in the Norwegian Sea on May 07, 2013 at position 65.67 N, 3.15 W, and represents conditions in the western Norwegian Sea in pre-bloom conditions, chlorophyll levels over the vertical profile peaked at ~0.9 mg $m^{-3}$. The second profile was obtained May 09, 2013, at position 67.05 N, 9.91 W, and shows conditions a little further west, also in pre-bloom conditions, chlorophyll levels over the vertical profile peaked at ~0.5 mg $m^{-3}$. The third profile was obtained in the Iceland Sea on June 07, 2013, at position 68.5 N, 10.75 W, and shows conditions for this area during a full bloom, chlorophyll levels over the vertical profile peaked at ~5.4 mg $m^{-3}$.

We used the vertical profiles of irradiance as input to a theoretical model of aquatic visual feeding (Aksnes and Giske, 1993), in order to actually assess habitat suitability to herring feeding. Visual range for a pelagic planktivore feeding on *Calanus finmarchicus* were parametrised following (Varpe and Fiksen, 2010):

$$r_{(t,d)}^2 e^{\left(c_{(r,d)} r_{(t,d)}\right)} = C_p A_p E' \frac{I_{(t,d)}}{K_e +} I_{(t,d)}, r \geq 0.05$$

$$r_{(t,d)} = \sqrt{C_p A_p E' \frac{I_{t,d}}{K_e + I_{(t,d)}}}, r < 0.05$$

Here $r_{(t,d)}$ is the visual range at time t and depth d, $c$ is the optical beam attenuation, $C_p$ is the prey contrast (0.3 (Aksnes and Utne, 1997),), $A_p$ is the prey image area ($3 \times 10^{-6}$ m for *Calanus finmarchicus,* Aksnes and Utne, 1997), $E'$ is the visual capacity, $K_e$ is a composite saturation parameter, and $I_{(t,d)}$ is the total organism perceived irradiance at time t and depth d. $E'$ and $K_e$ were scaled such that $r$ equalled 30 cm (e.g. 1 BL for an adult herring) when $c$ and $I$ were not limiting, following Varpe and Fiksen (2010). Details of the model can be found in Aksnes and Giske (1993), Aksnes and Utne (1997) and Varpe and Fiksen (2010). We did not modify the model, but modified the input parameters, such that irradiance and beam attenuation input to the model was weighted by the herring eye sensitivity spectrum. Herring eye sensitivity at wavelength was taken from Blaxter (1964), and scaled so that the sensitivity at the wavelength of maximum sensitivity (502 nm) was 1. $I_{(t,d)}$ thereby gives a measure of the light available to a herring eye, "herring-lux".

We estimated irradiance at depth, $I_{(t,d)}$ by first estimating wavelength specific attenuation coefficients, using wavelength specific underwater irradiances from the TriOS sensor:

$$k_{d(wi,d1)} = \frac{\ln\left(E_{(wi,d0)}\right) - \ln\left(E_{(wi,d0)}\right)}{(d0 - d1)}$$

To make the estimates of visual range more directly comparable between the areas, we used the same diel surface irradiance sequence to evaluate all 3 profiles, this diel sequence was constructed by 15 min averages of data points recorded in the period June 07, 2013–June 10, 2013. Wavelength specific irradiances at depth were then estimated from

$$E_{(wi,d)} = F \times E_{(wi,0)} \times e^{-\int_0^d k_{d(wi,0)} z dz}$$

where $E_{(wl,0)}$ is the above surface irradiance at wavelength wl, F is a factor used to account for the attenuation of irradiance when going from air to water (in this case arbitrarily set to 0.5). Total herring perceived irradiance (in photons $m^{-2}$ $s^{-1}$) were estimated as

$$I(t,d) = \sum_{wi=440}^{600} E_{(wi,d)} \times HerringSensitivity_{wi}$$

where $HerringSensitivity_{wl}$ is the spectral sensitivity of the herring eye, digitized from Blaxter (1964), and the (t,d) subscript denotes that this was done for each timestep (15 min) and depth (5 m resolution) bin. The final parameter needed for estimation of the visual range is the beam attenuation coefficient. We estimated these, per wavelength, from the following relations:

$$(a + b_b) \simeq \frac{K_d \times \mu}{1.04}$$

From Morel et al. (2007), where $a$ is absorption and $b_b$ is particle scattering, and $\mu$ is the average cosine of the angular distribution (here set to 0.82, Brown et al., 2004). Finally, the beam attenuation $c$, is the sum of absorption and scattering terms:

$$c = a + b$$

For input to the visual range estimations, an overall c was produced by weighting the wavelength specific beam attenuation coefficients by their *in situ* herring perceived light levels. Based on estimated visual ranges $r$, we then estimated potential searched volumes over the diel cycle:

$$volumesearched = 0.5x \times r^2 \times v \times t$$

where $v$ is swimming speed (2 BL $s^{-1}$, e.g. 60 cm $s^{-1}$, Varpe and Fiksen (2010) and $t$ is timestep.

## 3. Results

### 3.1. Hydrography, nutrients and chlorophyll along the MESSOR transect

The CTD data from the MESSOR tow along the transect from east towards west, 10–400 m depth, revealed two water masses, warm and saline Atlantic water in the east and cold and less saline Arctic water in the west (Fig. 2). At depths close to the surface, the position of the Arctic front was about 40 km from the eastern starting point. At about 150 m depth the front was located further west at about 50 km. The same pattern is seen in the data from the underway sensors sampling a water-intake at 4 m, both salinity and temperature data reveal a front between 40 and 50 km, surface temperatures east of the front are close to 7°, and surface temperatures west of the front just above 5 (Fig. 3). Over the front salinities dropped ~ 0.2 PSU east to west. The MESSOR data also showed that at the front, the denser Atlantic water was submerged under the Arctic water (Fig. 2). The uppermost layer of water had been warmed up due to insolation, forming a thermocline at 40–50 m depth

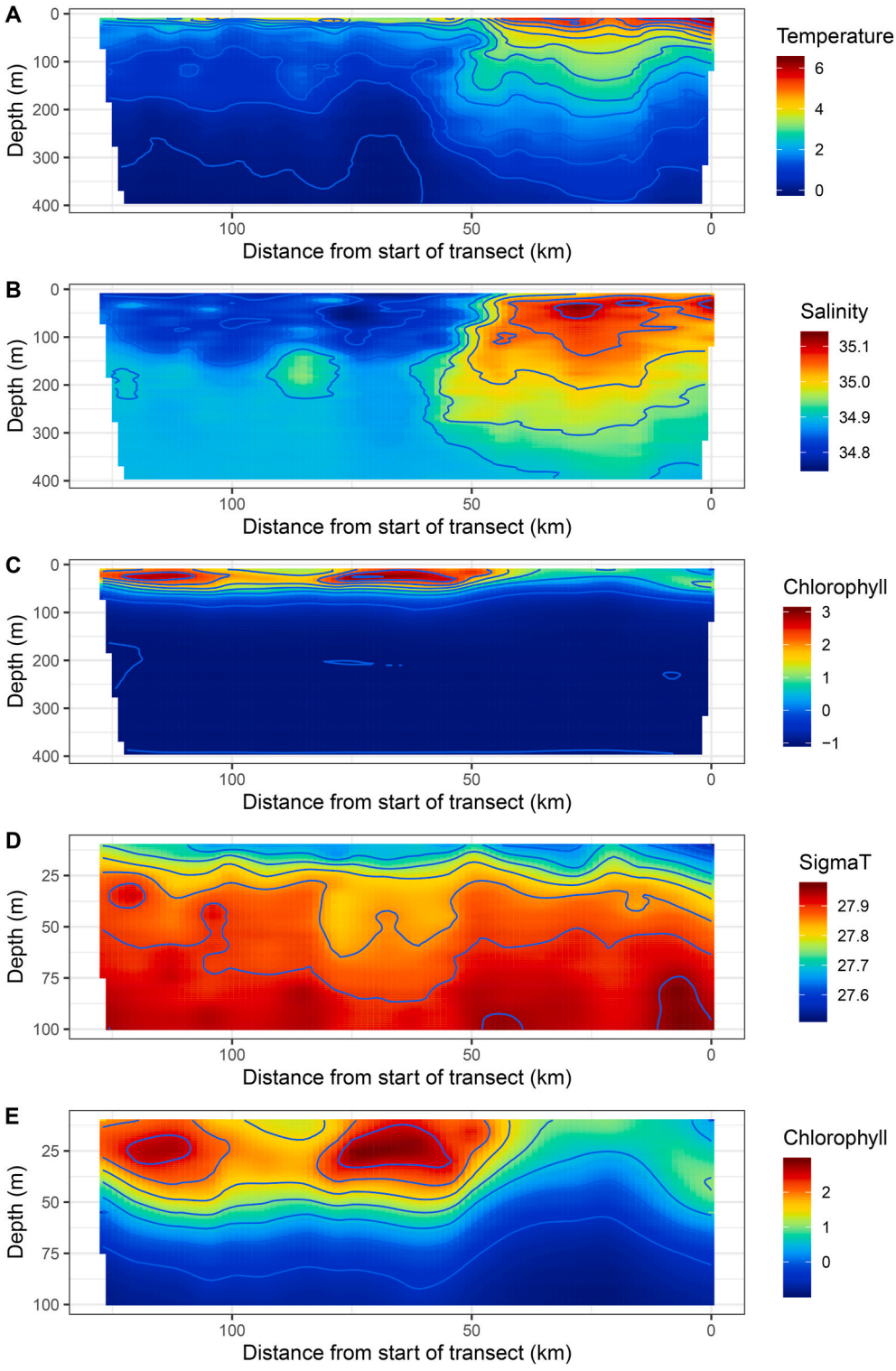


**Fig. 2.** Temperature (°C), salinity, water density (sigmaT) and chlorophyll (mg $L^{-1}$) along MESSOR transect (see red line in the map of Fig. 1). The transect starts at 0 km in the east, heading north-west. The Arctic front separates Atlantic and Arctic water masses at a salinity of about 35 (Fig. 1) and is located at 40 km near the surface and at 50 km at ~150 m depth. The fluorescence measured by the fluorometer was converted to chlorophyll concentrations (mg $m^{-3}$) using the relationship: *Chlorophyll* = 0.9036**Fluorescense*-0.9997 (Naustvoll et al., this issue). Upper panel: 0–400 m for T, S and chlorophyll. Lower panel: 0–100 m for sigmaT and chlorophyll. The lower panel is focused on the upper 100 m to show the existence of a shallow pycnocline along the whole transect and a deep chlorophyll maximum in Arctic water.

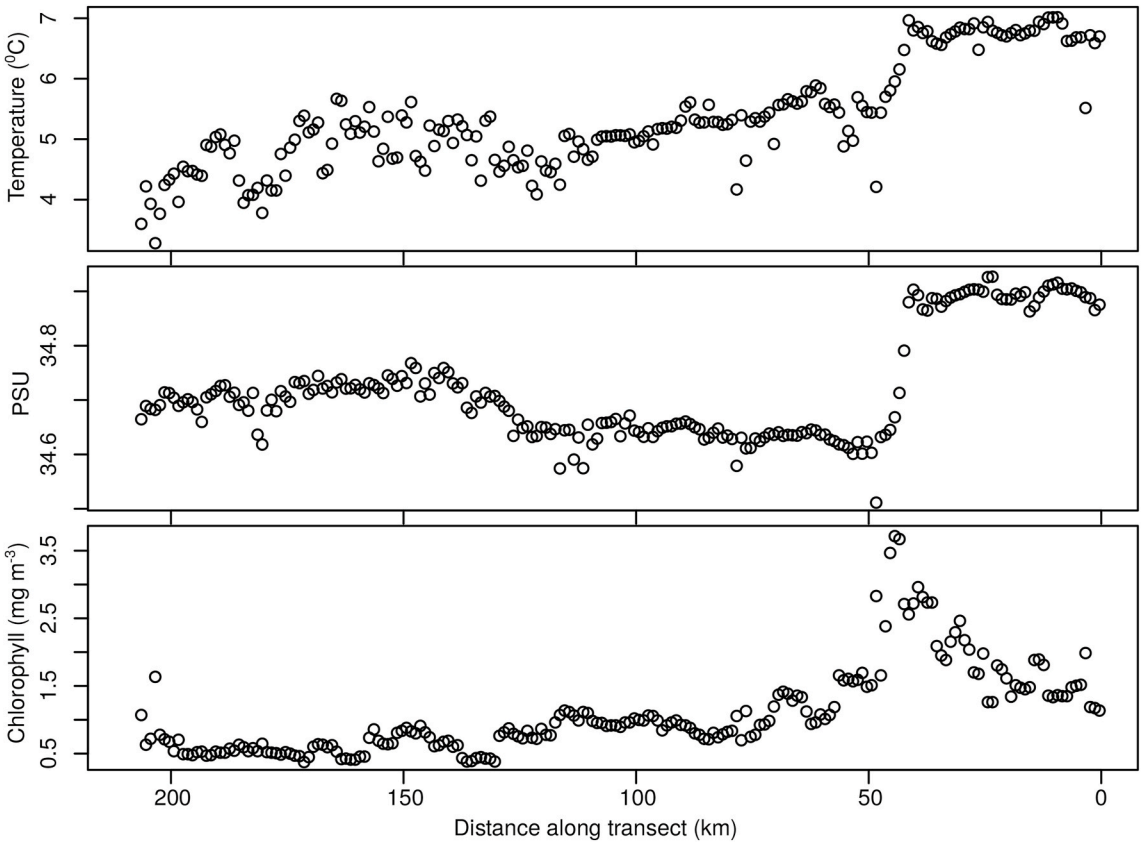


**Fig. 3.** Underway sensors plotted against distance (km). Upper panel: Underway sensor (8.5 m intake) minimum temperature per km. Middle panel: Underway sensor salinity (PSU) minimum salinity per km. Lower panel: Underway sensor maximum chlorophyll per km (mg $m^{-3}$). The Arctic front was located at 40–50 km from the start of the transect.

along the whole transect. On the eastern Atlantic side of the front, warm and saline Atlantic water was sitting on top of Arctic intermediate water, forming a deep additional pycnocline at ~200 m.

Fluorescence based chlorophyll measurements from the underway sensor show indications of a bloom in the surface waters just west of the salinity and temperature front (Fig. 3), which is not visible in the MESSOR data (Fig. 2), but then all MESSOR data above 10 m were removed before analysis. Towards the start of the transect chlorophyll levels were close to 1 mg $m^{-3}$ at the surface. In the bloom area values reached ~3.5 mg $m^{-3}$, whereas values west of the bloom were very low, coming close to 0.5 mg $m^{-3}$ in the far west (Fig. 3). Fluorescence measured by the MESSOR tows revealed a deep chlorophyll maximum at a depth of about 30 m on the Arctic side of the front (Fig. 2). The fluorescence peaked in two areas just west of the front and towards the end of the transect. Fluorescence in the Atlantic water was lower, and a sub-surface maximum was not clearly identifiable (Fig. 2). 7 CTD stations starting a 0 km along the MESSOR transect and ending at 200 km (Fig. 4) showed that the chlorophyll was peaking at about 20 m close to the front on the Arctic side. Chlorophyll concentrations were low in Atlantic water and towards the end on the Arctic side. Nitrate and silicate concentrations in the upper 25 m were low, overall (Fig. 4), while towards greater depths the concentrations were higher. On the Atlantic side the nutrient concentrations at depth were lower than on the Arctic side.

### 3.2. *Mesozooplankton, micronekton and herring along the MESSOR transect by net, optic and acoustic observations*

The stage distribution of *Calanus finmarchicus* along the transect, based on four MOCNESS hauls, two in Atlantic water, one near the front, and one in Arctic water, showed that the older stages, CV and adults, dominated at all stations. Copepodite abundances ranged from ~10 to ~1500 ind. $m^{-2}$. Somewhat elevated density of stage CI (~1500 ind. $m^{-2}$) was found at a single station in Atlantic water, indicating that reproduction and recruitment to copepodite stages had commenced (Fig. 5). CII and CIII did not show higher abundances compared to other stations.

In terms of densities of objects estimated by the OPC on MESSOR, size classes 2 and 3, the objects smaller than and equal to the size of copepodites II and III of *Calanus finmarchicus* (Table 2), peaked in the upper 70–80 m (Fig. 6). Densities of small particles, ie. size class 2, were higher in Atlantic water, while densities of size class 3 particles were higher in the Arctic water. Size class 4 was not observed near the surface in Atlantic water and peaked at about 50 m in Arctic water (size similar to *C. finmarchicus* CIV). Size classes 5 (size similar to *C. finmarchicus* CV and CVI) and 6 (Table 2) were distributed similarly to size class 4, with lower abundances and a deeper distribution in Atlantic water. Size class 6 also had much lower densities in the Atlantic water, and may have migrated below 400 m during daytime in the east (Fig. 6, sun elevation in upper left panel). Two high density regions (in size classes 4 and 5) below 300 m on the Atlantic side of the front were interpreted as belonging to a different taxonomic group than the particles observed in surface waters (see VPR results).

All acoustic categories showed a pattern consistent with diel vertical migration, with deeper distributions observed during the day in Atlantic water than at night in Arctic water (Fig. 7). However, since we also crossed the front, it is possible that spatial and temporal vertical patterns are confounded. For the category with the highest backscatter at the highest frequencies, we observed only limited backscatter in the upper ~150 m during the day, whereas peak backscattering levels were observed in the upper 100 m at night in Arctic waters. This pattern is similar to the vertical distribution changes that we observed in OPC particle size 5 and to some extent size 6.

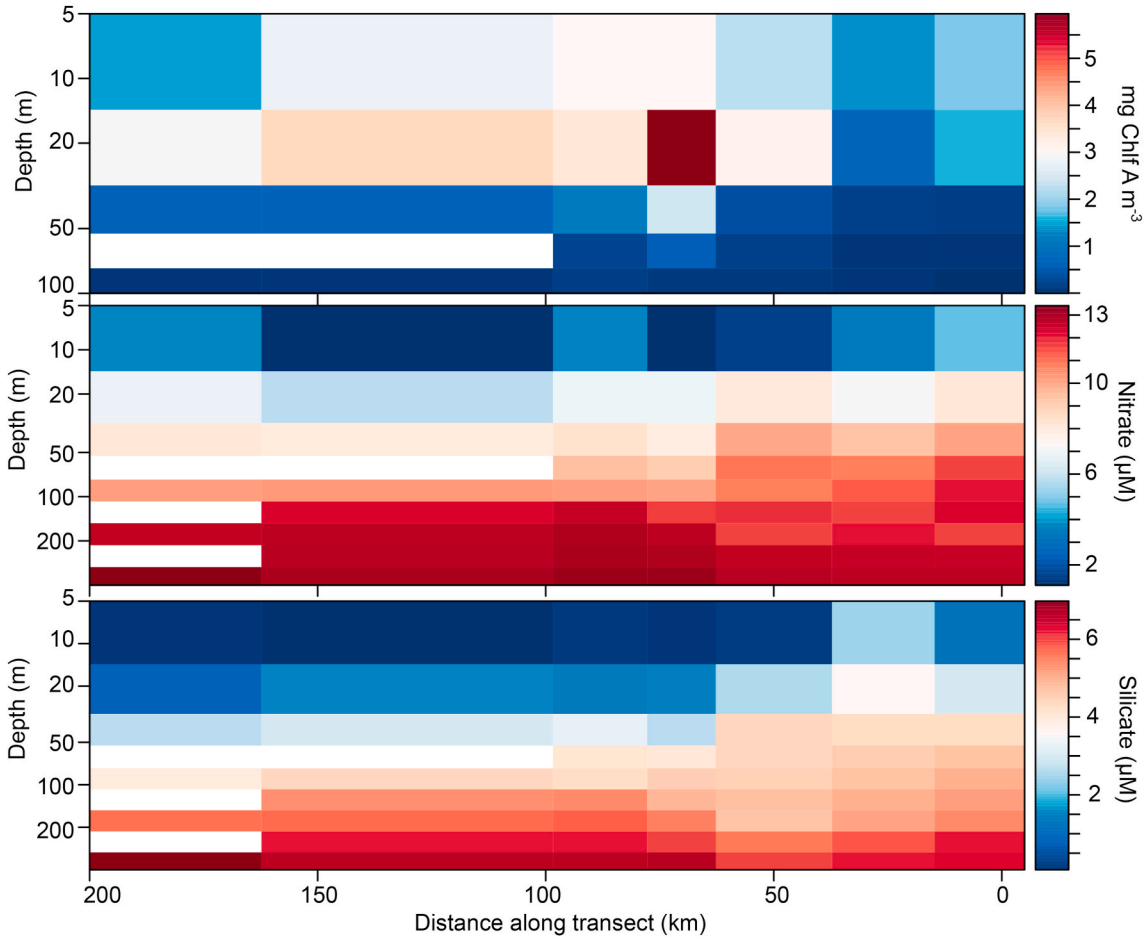


**Fig. 4.** Chlorophyll (mg $m^{-3}$, upper), nitrate (µM, centre), and silicate (µM, lower) concentrations versus depth and distance along an extended transect. 0 km denotes the start of the MESSOR transect. The Arctic front was located at 40–50 km from the starting point. Water samples were collected by water bottles mounted on a CTD. Note that vertical scale is compressed at depth to highlight the shallow water where the strongest gradients were found. Maximum depth displayed for chlorophyll and nutrients are 100 and 300 m, respectively.

In the VPR data, female copepods with egg sacs were largely found in Arctic water, peaking at about 150 and 300 m depths in the VPR (Fig. 8). In the MOCNESS samples we found most *Pseudocalanus* females in the upper 25 m, but all adult females noted to carry egg sacs, such as *Pareuchaeta,* were found below 250 m (data not shown). The *Pareucheata* females were rare in the MOCNESS samples. The copepods as a group were dominated by *Calanus* spp. (data not shown), but it was not possible to separate the latter as a statistically significant group in the VPR images. VPR derived estimates of copepod densities were highest in Atlantic water, with a bimodal distribution with centres at ~50 and 200 m. The highest densities of marine snow particles were observed below 200 m in Atlantic water, and from ~50 to 225 m in Arctic water (Fig. 8). A high proportion of the marine snow particles were identifiable as faecal pellets of copepods (Voss, 1991).

MOCNESS stations showed that mesozooplankton densities were highest in the upper 25 m (Fig. 9) peaking at more than 60 000 ind. $m^{-3}$. One station at 25 km from the eastern starting point of the transect showed only half the densities observed at the other three stations, peaking at 30 000 ind. $m^{-3}$. The abundances equals the sum of all taxa in the eight depth intervals per station excluding the smallest taxa like eggs and copepodites I and II. The reason for not showing the distribution of every species is that the main purpose of Fig. 8 is to show the difference in vertical distribution of the herring's prey species (see Fig. 14) compared to the total mesozooplankton community.

In the macroplankton trawls catches the same taxa occurred on both sides of the Arctic front, except for the gastropods (Fig. 10). Six of ten taxa occurred with the highest biomass in Arctic water. Amphipods, copepods, cephalopods, decapods, and gelatinous plankton abundances peaked in the Arctic water. Krill, myctophidae and teleostei (e.g. smaller pelagic fish and fish larvae) occurred with highest biomass in Atlantic water.

The acoustic surveys of the transect line (the transect was surveyed twice to map the distribution of herring while also sampling with nets and CTDs) showed that the herring were distributed along most of the transect, except for the 30 westernmost kilometres (Fig. 11 A). In the eastern parts of Atlantic water, the herring occurred only in the upper 50 m. Further west, in the frontal areas and the Arctic water, the herring occurred both near the surface and at depths down to 300 m. In contrast to some of the organisms observed by MESSOR acoustics, OPC, and VPR, the herring did not show a pronounced DVM pattern, and were found at depth both during day and night west of the front, and only in surface waters during daytime east of the front (Fig. 11 B). Length and weight of the herring in the trawl catches did not show a spatial trend (Fig. 12). Neither did fat content or condition factor (not shown).

### *3.3. Stomach content of herring, vertical distribution of their prey and modelled light by depth*

Stomach contents of the herring was highest in Arctic water, ranging from 0.9 to 1.1 g per stomach, and lower in the frontal region and in Atlantic water, ranging from 0.3 to 0.5 g per stomach (Fig. 13). The dominant prey at all stations were copepods of the genus *Calanus*.

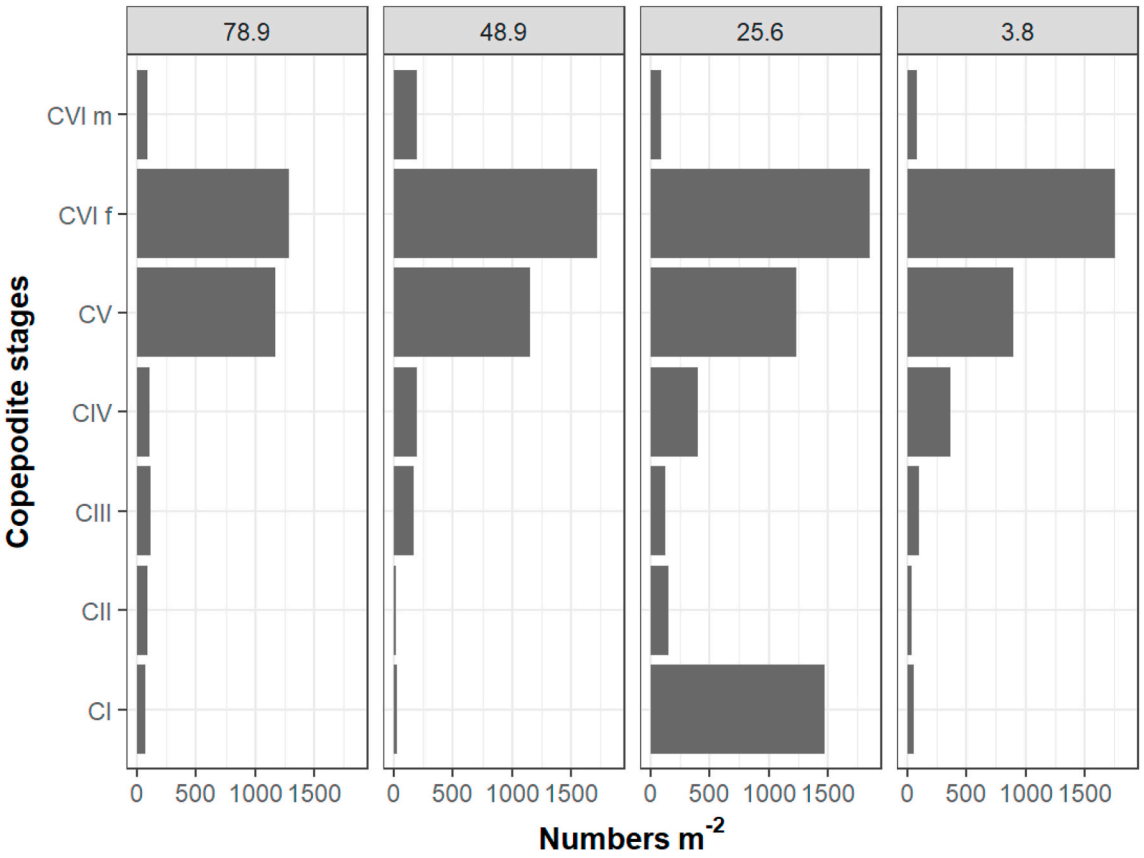


**Fig. 5.** Stage distribution of *Calanus finmarchicus* at four MOCNESS stations. Numbers on x-axis are surface integrated densities over the 400 m depth interval that was sampled. Numbers on top of each panel are distance from start of the transect (km). The Arctic front was located at 40–50 km. CI to CV, denote the first five copepodite stages. CVI f, denotes adult females. CVI m, denotes adult males.

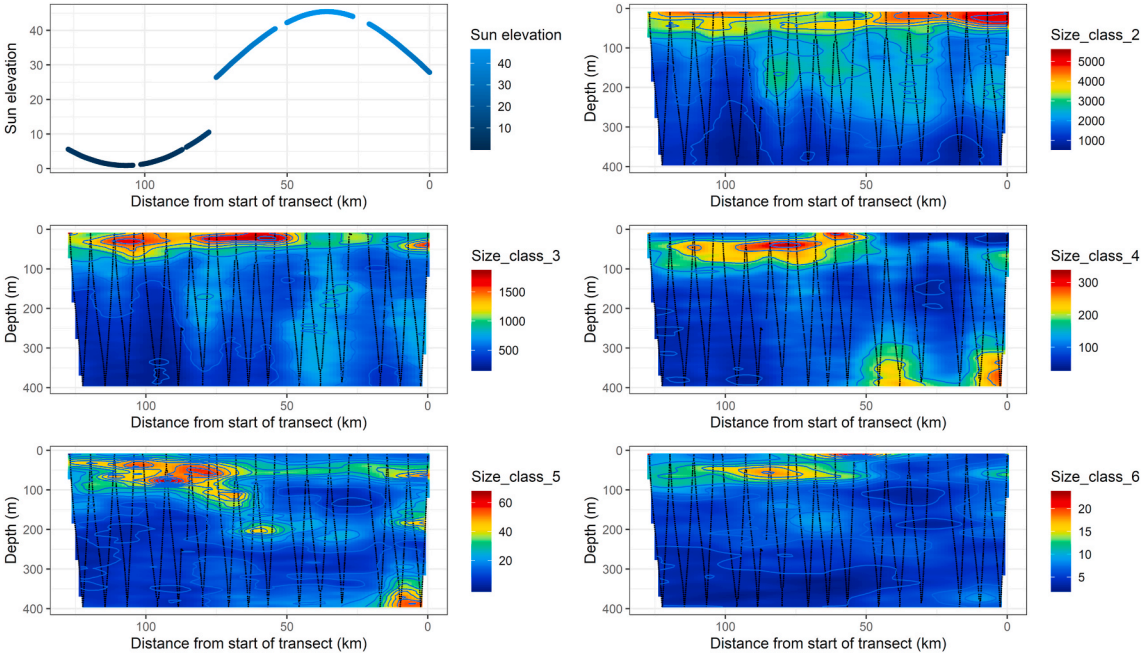


**Fig. 6.** Horizontal and vertical distribution of particle size classes (ESD) from OPC on MESSOR (Nos $m^{-3}$). Upper left panel shows sun elevation as degrees above horizon. The Arctic front is situated at 40–50 km.

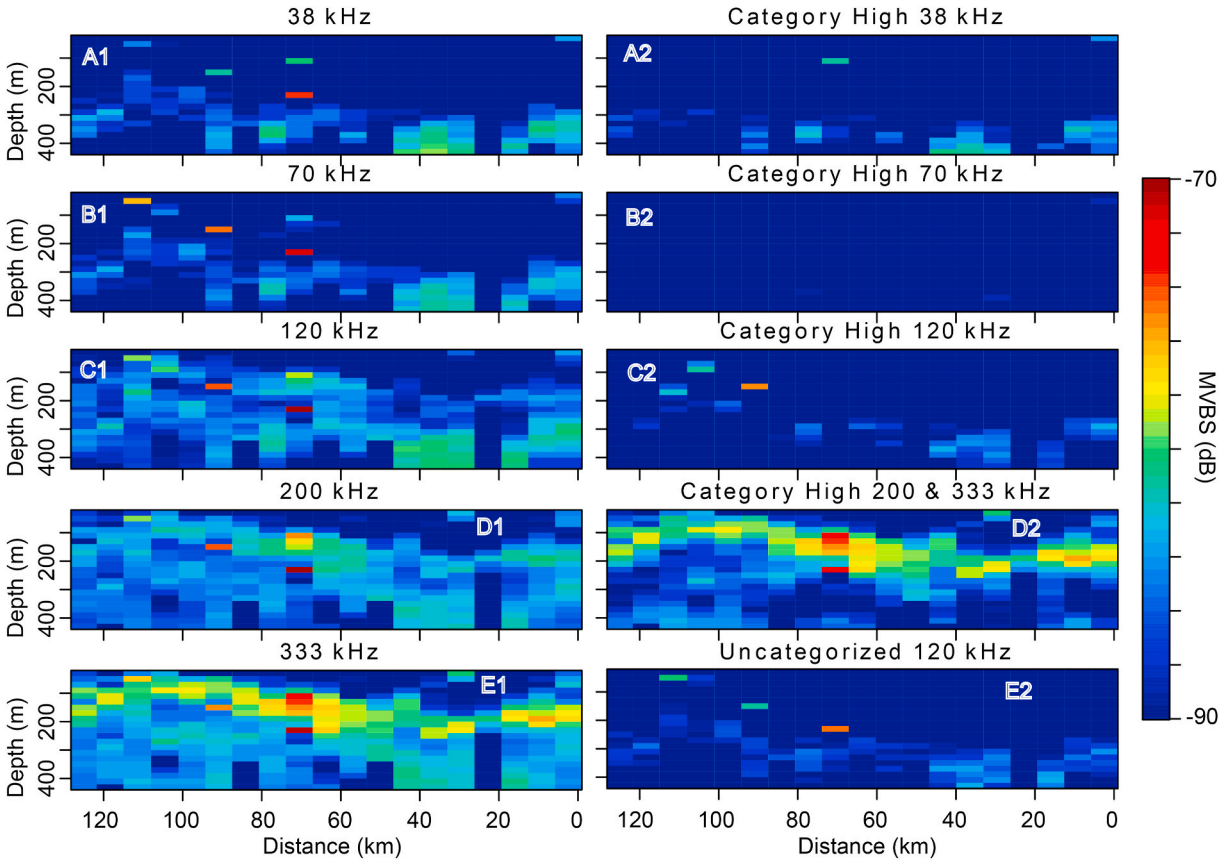


**Fig. 7.** Binned multifrequency data (A1-E1) and backscatter assigned to acoustic categories from MESSOR multifrequency acoustics (A2-B2) plotted against distance along transect and depth (m). The Arctic front was located at 40–50 km.

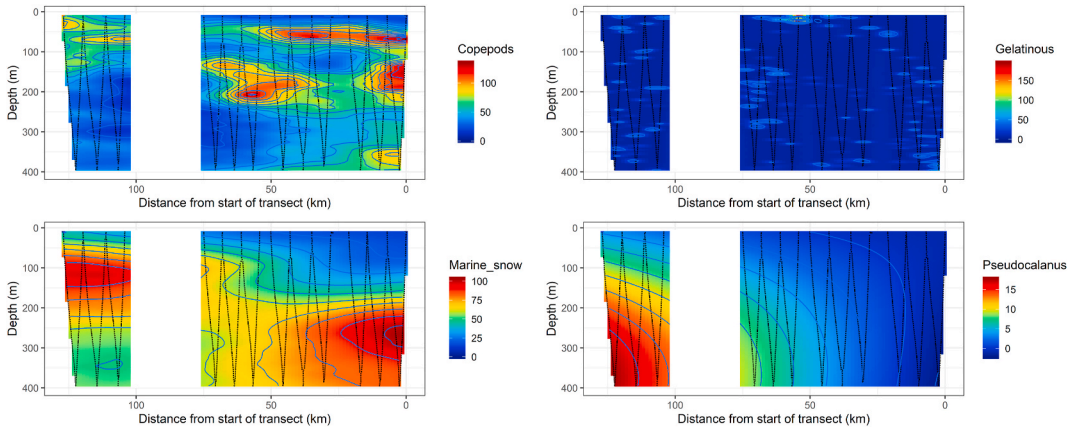


**Fig. 8.** Distribution of taxa in VPR on MESSOR (Nos. $m^{-3}$). The white box represents a region of lost VPR data. The Arctic front was located at 40–50 km.

*C. finmarchicus* dominated stomach contents in Atlantic water, *C. hyperboreus* and the copepod *Metridia* being more dominant in the Arctic water masses. In Arctic water, also the Euphausiidae (krill) and *Themisto* (amphipods) were important prey.

Vertical distributions of mesozooplankton from the MOCNESS samples showed a shallow distribution, with most organisms occurring near the surface (Fig. 9). The vertical distribution of the prey items of the herring was shifted towards larger depths (Fig. 14) relative to the overall vertical numerical distribution (Fig. 9). Sun elevation at the time of sampling showed that one station was sampled during twilight (the second westernmost station), while the others occurred during the day (Fig. 14). During daytime, important prey like *Metridia* had peak densities at depths below 100 m, with the vertical distribution extending down to the maximum depth we observed herring, at ~300 m. Important prey like *Calanus* species, amphipods (*Amphipoda*), and krill (*Euphausiacea*) were most abundant in the upper 25–50 m, and also *Calanus* spp. showed a shallower distribution at the twilight station. The upward shift in peak densities for *Metridia* during twilight was ~100 m, for *Calanus* spp. the upward movements were within the upper 75 m or less. For the smaller copepod species, e.g. *Microcalanus*, an upward shift in density was not observed.

During the period of main sampling, we measured optical conditions under either post-bloom (in the east) or late-bloom conditions (in the west). In order to compare with pre-bloom conditions, we added optical

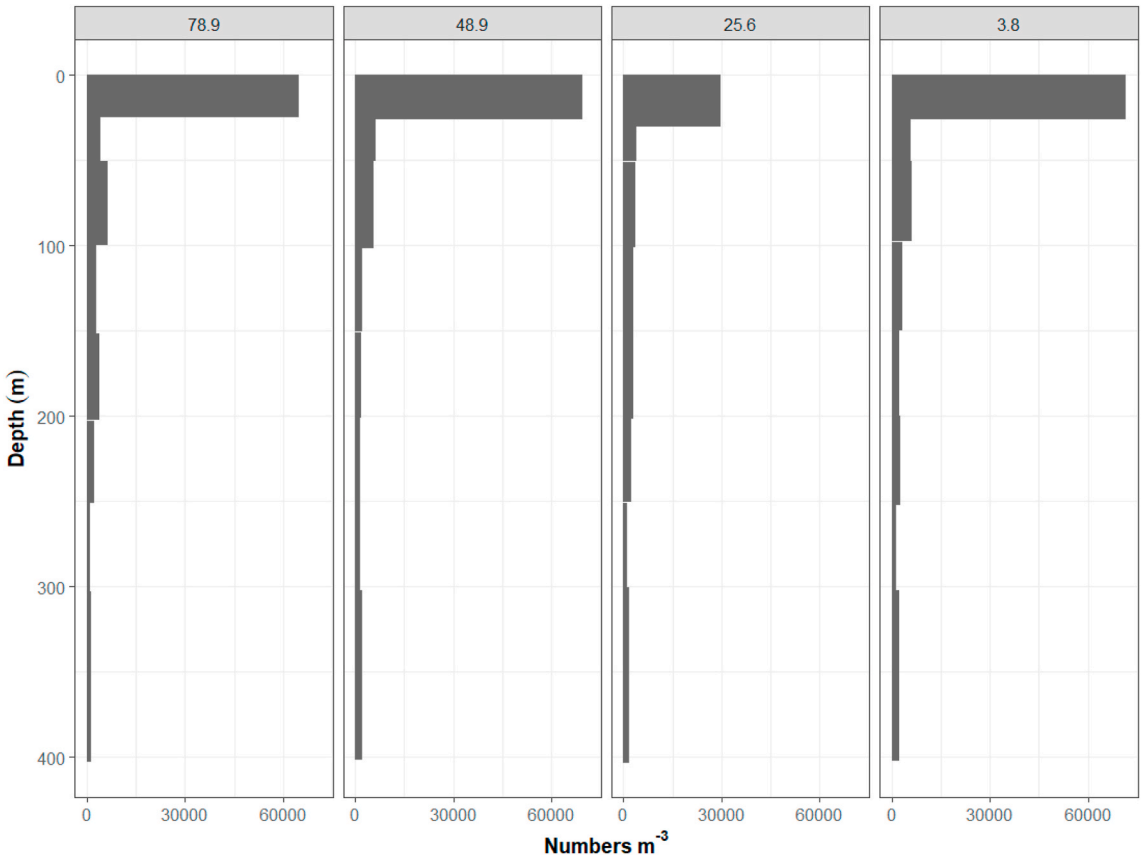


**Fig. 9.** Vertical distribution of zooplankton taxa in the MOCNESS samples (Nos. $m^{-3}$), excluding copepod eggs, nauplii and copepodites stages I to III. Numbers on top of each panel are distance from start of the transect (km). The Arctic front was located at 40–50 km. The sun elevation (degrees above horizon) at the time of sampling was 22, 40, 0.5 and 35° for the four MOCNESS stations from east towards west (right to left in the figure), respectively.

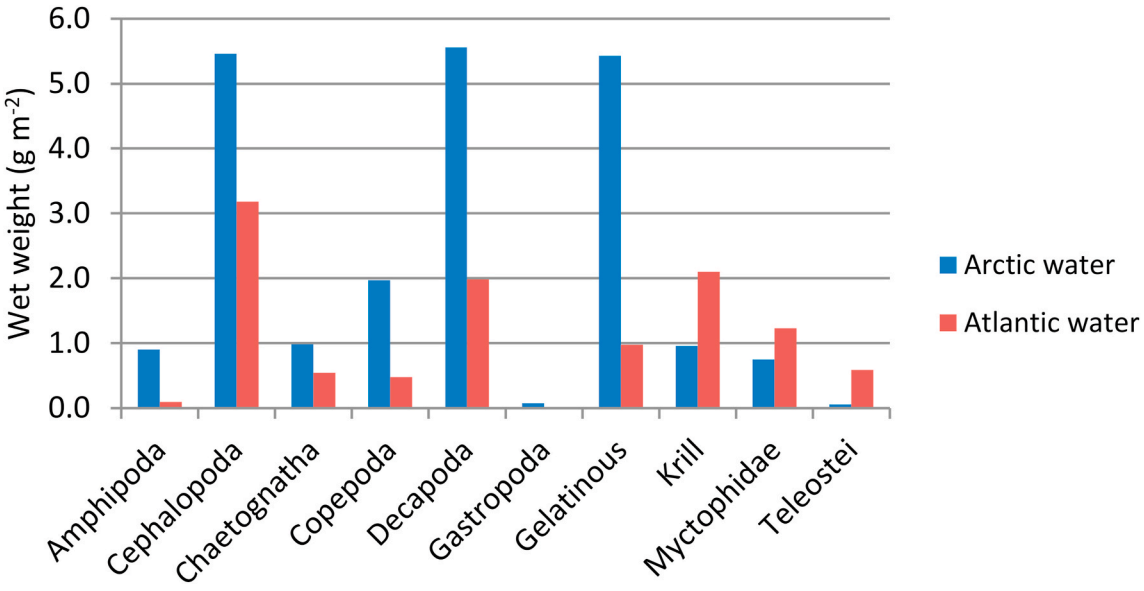


**Fig. 10.** Biomass of macroplankton and micronekton (wet weight, g $m^{-2}$) from Macroplankton trawl V-hauls, 0–400 m in Arctic and Atlantic water. The trawls were located outside the range of the MESSOR transect. Position of trawls are given in Fig. 1.

data collected a month previous, in early May, during the transect to Iceland. Under late-bloom conditions in the western part of the transect (7 June), measured light levels at 40 m was lower by more than 1 order of magnitude compared to pre-bloom conditions in the Iceland Sea (Fig. 15 A). The highest light penetration to depth was measured in the Iceland Sea, prior to bloom conditions (e.g. using the 9 May 2013 profile), but light penetration at 40 m was superficially similar in the Norwegian Sea prior to the bloom (e.g. 7 May). However, even if measured light levels at 40 m looked superficially similar in the early May measurements, the modelling suggested that the differences in light

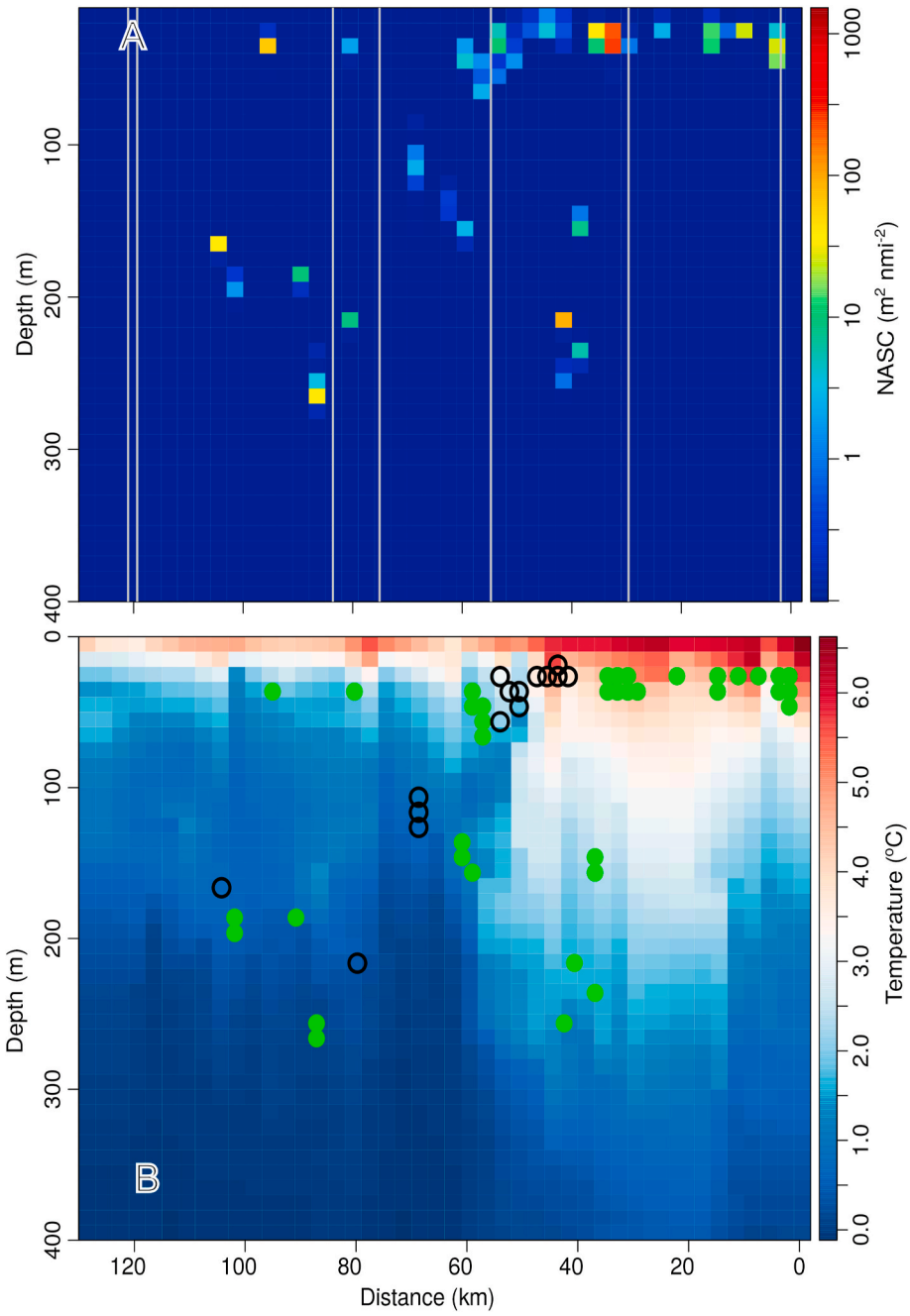


**Fig. 11.** Distribution of herring. A: Acoustic backscatter attributed to herring (38 kHz volume backscatter (NASC)) plotted against distance along transect and depth (m), with vertical grey lines indicating positions of trawls. B: Day (green points) and night (black circles) distribution of herring, overlaid on *in situ* temperature recorded from MESSOR. The acoustic data are composites for all traverses of the transect line and were therefore recorded over a longer timespan than the MESSOR data. The Arctic front was located at 40–50 km.

attenuation would result in relatively large differences in potential searched volume (Fig. 15 B), under the same surface illumination regime. Close to the surface the magnitude of these differences was relatively minor, with relatively larger differences found at depth. Under bloom conditions, the model predicted negligible search volumes deeper than 40 m, for a herring searching for a *Calanus finmarchicus* type prey (Fig. 15 B), but even the Norwegian Sea profile pre-bloom showed reductions in potential search volumes of >500 $m^3$ per day compared to Iceland Sea pre-bloom deeper than ~ 30 m.

## 4. Discussion

### 4.1. Horizontal patterns in herring stomach contents

Herring stomach contents were higher towards west (Fig. 13). Horizontal distribution of the herring during its feeding migration has been explored in relation to both food and temperature (Misund et al., 1997; Fernö et al., 1998; Kvamme et al., 2003; Nøttestad et al., 2007Broms et al., 2012). Broms et al. (2012) concluded that food availability was the major driver for the herring migration, and that the herring movement towards lower temperatures was a consequence of following gradients in the prey distribution.

The differences in herring stomach contents were mirrored in the occurrences of the larger size groups in the OPC data, which were also higher in the west. These larger size classes span the sizes of the most important prey species of herring (Fig. 13). This pattern of higher densities in the west was not obvious in the MOCNESS and VPR data, but these instruments had either very few hauls (MOCNESS) or sample a very small volume (VPR).

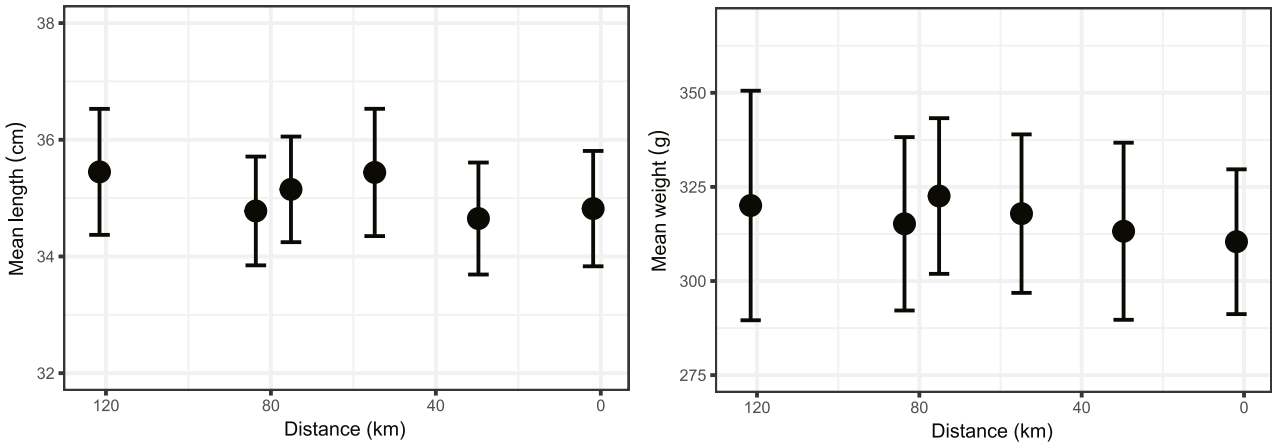


**Fig. 12.** Mean and SD of total body length (cm) and total body weight (g) of herring in 6 Multpelt trawl catches along the transect. The Arctic front was located at 40–50 km from the start of the transect. Position of hauls are given in Fig. 11.

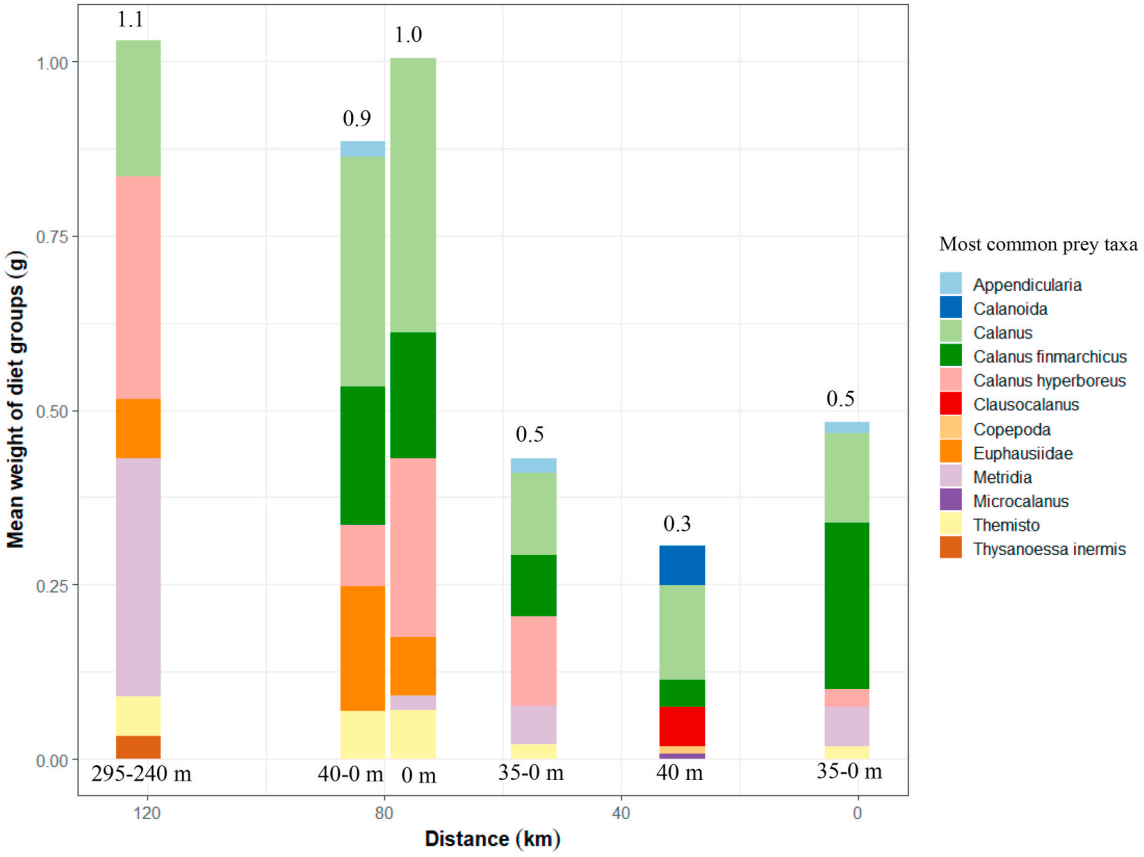


**Fig. 13.** Herring diet. Mean dry weights (g) of the 12 most common prey organisms per herring stomach over all trawl stations. Average total stomach content dry weights (g) per trawl station are given on top of each column. Below each column the smallest and largest sampling depths (m) of the trawl stations are given. The Arctic front was located at 40–50 km from the transect starting point at 0 km.

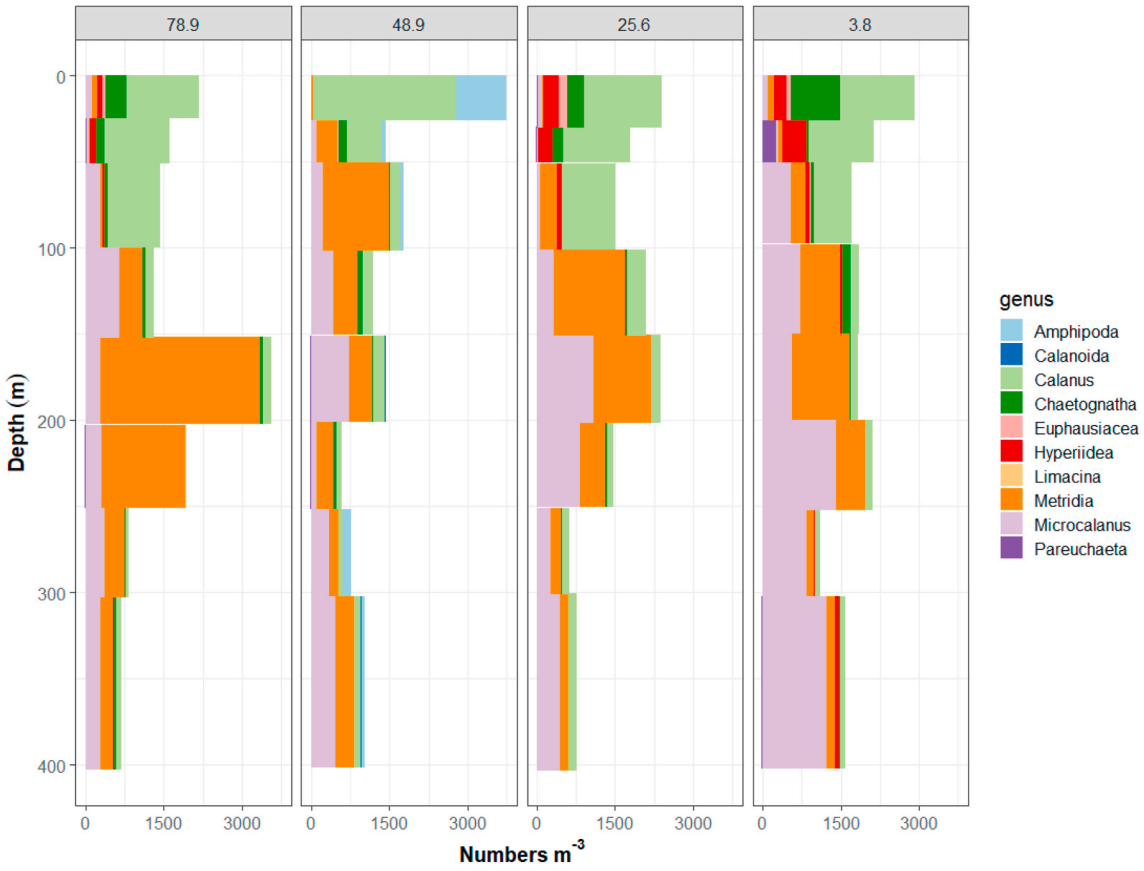


**Fig. 14.** Vertical distribution of herring prey (Nos. $m^{-3}$) in MOCNESS catches, for categories of prey found in herring stomachs. Numbers at the top of each panel is distance in km along the transect. The sun elevation (degrees above horizon) at the time of sampling was 22, 40, 0.5 and 35° for the four MOCNESS stations from east towards west (right to left in the figure), respectively. The Arctic front was located at 40–50 km from the starting point of the transect.

### *4.2. Phenology of phytoplankton and calanus in relation to the herring migration*

The data from continuous near surface measurements of temperature, salinity and fluorescence; chlorophyll, silicate and nitrate concentrations from 7 CTD stations encompassing the MESSOR transect; and temperature, salinity and fluorescence from the MESSOR tows told the same story - there was a deep bloom going on at the depths of the pycnocline in Arctic water, while in Atlantic water and in the mixed surface layer of Arctic water chlorophyll concentrations were low. The nutrients, represented by silicate and nitrate, were spent in both Arctic and Atlantic surface waters, and nutrients were lower in deeper waters (e.g. > 100 m) in Atlantic water compared to Arctic water. We interpreted this as phytoplankton bloom development being more evolved in Atlantic water than in Arctic water, since when nutrients are fully spent in the mixed layer, low chlorophyll concentrations indicate that the bloom is over. Deep chlorophyll concentrations are an indication of late blooms (Rey, 2004). Thus, we would classify the phytoplankton development in Atlantic water as a post-bloom situation and in Arctic water as late-bloom situation. The alternative interpretation that the bloom has not started in Atlantic water does not comply with the spent nutrients that we observed there. However, the bloom in Atlantic water is known to never display high levels of chlorophyll (Rey, 2004), so an alternative interpretation could be that we just observe two different types of bloom dynamics in the two water masses. The bloom development in both water masses are driven by the shallowing of the seasonal thermocline, and we do see a shallow thermocline in both water masses (see also Drinkwater et al., this issue). Atlantic water is usually reported to have higher winter nutrient concentrations than Arctic water (Rey, 2004). The lower concentrations of nutrients at depth in Atlantic water compared to Arctic water, thus indicates that the total use of nutrients by the phytoplankton in Atlantic water was higher than in Arctic water, also indicating a longer productive period or more intense bloom there. This is supported by large scale investigations of the bloom dynamics of the Norwegian and Iceland Seas stating that there is a south-east to north-west gradient in phytoplankton phenology, starting in the south-east with a delay of several weeks towards north-west (Rey, 2004; Erga et al., 2014).

Copepodite stage distribution of *Calanus finmarchicus* is related to the phenology of the phytoplankton (Broms et al., 2007, 2012; Bagøien et al., 2012). *C. finmarchicus* overwinter in copepodite stages IV, V, and VI. From late winter to early summer, dependent on water masses and environmental conditions, the overwintering stages return to the surface waters to feed and reproduce (Melle et al., 2004; Broms et al., 2007; Bagøien et al., 2012). The reproduction of *C. finmarchicus*, or more precisely the recruitment to the first copepodite stage generally coincides with the peak in chlorophyll during the vernal bloom in the eastern and central Norwegian Sea (Melle et al., 2004; Broms et al., 2007). Stenevik et al. (2007) showed that the egg production of the *C. finmarchicus* population of the Norwegian Sea was highest during the pre-bloom phase due to the presence of many females, second highest during the bloom due to high individual egg production rates, and lower during the post-bloom phase. As the phytoplankton bloom development spread from southeast towards northwest in the Norwegian and Iceland Seas, the peak in *C. finmarchicus* reproduction follows the same pattern (Broms et al., 2007, 2009; Bagøien et al., 2012). Broms et al. (2012) showed that number of CV of *C. finmarchicus* did not start to increase due to the recruitment to G1 (the first generation of the year) until late June and early July. Gislason and Astthorsson (2002) also pointed to June and July as the period of maximum recruitment to G1 CV in the waters near

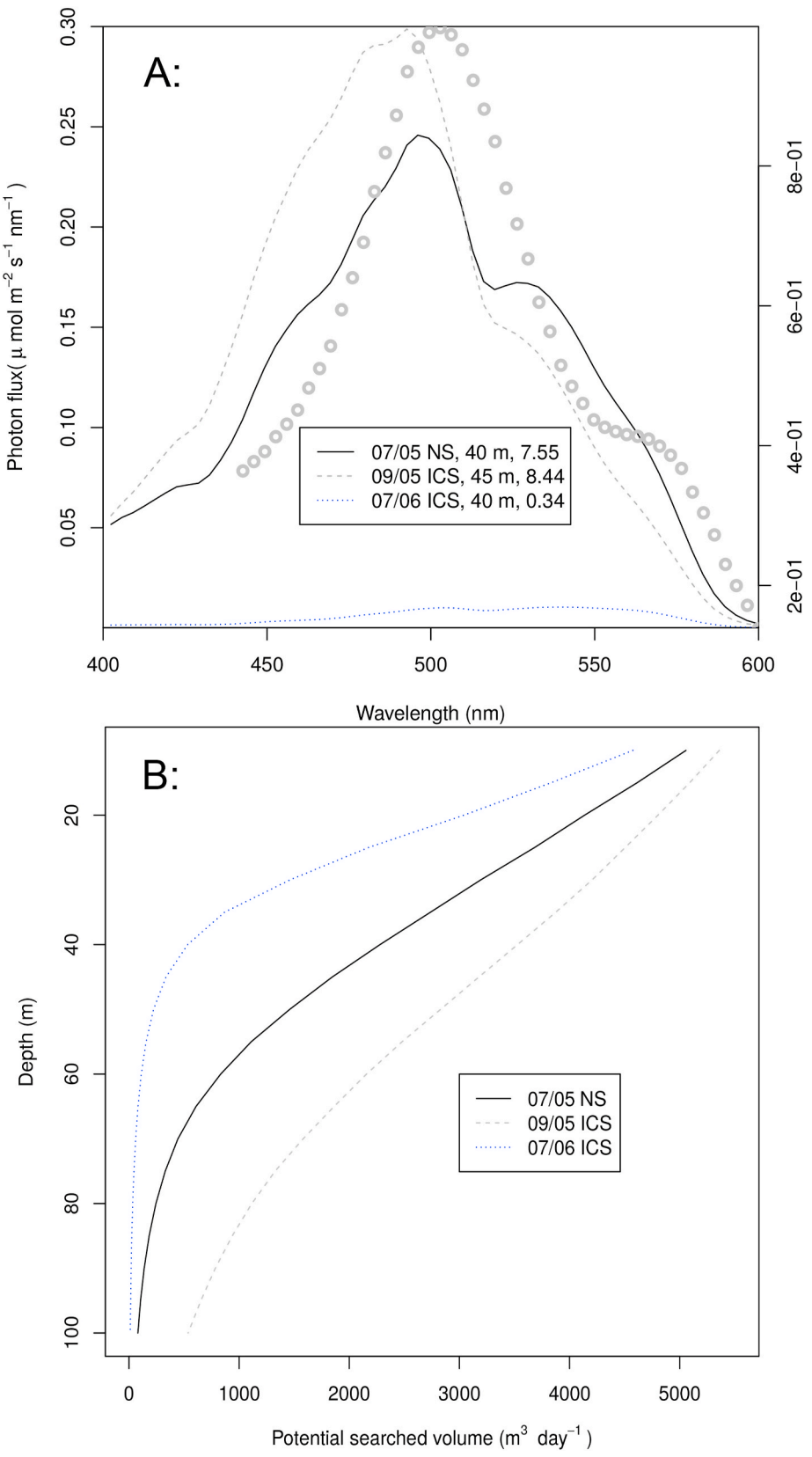


**Fig. 15.** A: Measured *in situ* light spectra from the Norwegian and Iceland Seas, at around 40 m depth. The two first spectra are from pre-bloom situations (recorded in early May, prior to the other data presented, chlorophyll maximum levels respectively 0.9 and 0.5 mg m$^{-3}$), whereas the last spectrum are from a bloom situation, with maximum chlorophyll levels > 5 mg m$^{-3}$. Superimposed on the measured light spectra are the estimated spectral sensitivity of herring (grey circles), based on Blaxter (1964). Legends give date and depth of measurement, as well as integrated light intensity (400–600 nm), in units of µmol photons m$^{-2}$ s$^{-1}$. B: Modelled potential search volume per day, plotted against depth. The modelling is based on a theoretical model of visual feeding, measured vertical profiles of light attenuation, and measured surface irradiances in the period June 07, 2019 to June 10, 2019, for details see text.

the Arctic front. Broms et al. (2009) stated that young copepodites of the new generation seemed to be tuned to the phytoplankton bloom in Atlantic water proper (eastern Norwegian Sea), while its development was delayed in Arctic water, so that the young of the year did not match the timing of the phytoplankton bloom. If we are right that the states of the blooms in Arctic and Atlantic water were post-bloom and late blooms, respectively, we also observed a delayed development of G1 compared to the situations in the eastern Norwegian Sea. Thus, the CIV,

CV, and adults of *C. finmarchicus* on the transect in this study should be of G0 (the overwintering generation), in both Arctic and Atlantic waters. At one station east of the front, some CI were observed indicating that G1 had recruited to copepodite stages. Based on previous observations of pre-bloom spawning it is reasonable to assume that eggs and nauplii were present in the area, but the MOCNESS equipped with 180 μm nets would not sample the small organisms effectively.

Broms et al. (2012) show how the feeding migration of the herring is timed to the phenology of seasonal vertical migration, reproduction, and recruitment of *C. finmarchicus,* which in turn are related to the phenology of the phytoplankton vernal bloom on a basin scale. They reported that peak herring and *C. finmarchicus* G0 densities (CV and CVI), co-occurred in time and space. What Broms et al. (2012) observed on a basin scale and used statistical analyses to reveal, is also what our results suggest on a very fine scale. Although we can not identify the peak densities of the herring and the G0, we observed that herring preceded the G1 (first generation of the year) along the entire transect (e.g. the only elevated densities of G1 observed in our data are as CI on the MOCNESS station 25.6 km from the start, Fig. 5).

The shift from G0 to G1 via younger stages (that the herring do not feed on) is an annually recurring phenomenon of *C. finmarchicus's* phenology that also has a spatial pattern. The timing and direction of the herring's feeding migration may be an adaptation to this, or the herring can potentially use the increased abundances of G0 to navigate on a fine local scale, as discussed by Fernö et al. (1998) and Broms et al. (2012). If the relative stage composition from our MOCNESS catches are representative, there would be very little gradient in the stage composition across our transect, though of course the OPC data shows the existence of a numerical gradient (Fig. 6).

The abundances of the *C. finmarchicus* G0 stages, CIV, CV, and CVI, summed up to 2000–4000 individuals $m^{-2}$ (Fig. 5) in the MOCNESS catches across all stations. This is an order of magnitude less than typical peak abundances of the G0 in the central and eastern Norwegian Sea (Melle et al., 2014), indicating that the abundances of the G0 may have been reduced compared to the initial numbers arriving in surface waters after overwintering. It has been shown that reproduction coincides with a period of high mortality, probably related to predation (Melle and Skjoldal, 1998). The relatively low Calanus abundances may explain why the maximum herring stomach content peaked at only 1 g dry weight (Fig. 13), while at the peak of feeding more than 3 g average stomach content weight has been observed in other studies in the same geographical area (Broms, 2007). Both the low copepod densities and the low stomach contents indicate that feeding conditions near the front at the time of this investigation were not optimal. The feeding conditions may have been better in the west. There stomach contents were higher, and abundances of potential prey organisms, such as larger particles estimated by the OPC and the biomass of larger zooplankton and micronekton caught in the Macroplankton trawl, higher. On the other hand, the elevated stomach contents in the western area may also be related to the change in vertical distribution and behaviour of the herring and its prey. The low temperature on the cold side of the front will also slow down the digestion time and thus the turnover rate of food in the stomach.

### 4.3. Prey vertical distribution and herring feeding

The MESSOR deployment in the western area was during night (such as night is at high latitudes during that time of year), and both the VPR and the OPC estimates suggested that higher densities of organisms in the mesozooplankton size range were encountered closer to the surface. For the eastern areas, our results suggest that larger mesozooplankton are absent from the upper water during daytime. Despite being confounded by different water masses being covered during different periods of the day, vertical distributions in the OPC (Fig. 6) and VPR data (Fig. 8) suggest upward shifts in centres of abundance during night, consistent with DVM of mesozooplankton. Also, the hull mounted (e.g. Klevjer et al., this issue) and MESSOR echosounder data (Fig. 7) suggests DVM for the organisms with peak backscatter at high frequencies (e.g. 200 and 333 kHz). The backscatter for category 333 will be heavily influenced by organisms larger than the acoustic wavelength (~4.5 mm at 333 kHz, ~7.5 mm at 200 kHz). For organisms smaller than the wavelength, backscatter is predicted to rapidly fall with diminishing sizes, though smaller organisms will make a contribution especially if their densities are high, or if they have high acoustic impedances (e.g. air-inclusions). Backscatter for category 333 is therefore likely to be dominated by organisms toward the larger size range of mesozooplankton (e.g. > 4.5 mm), and macroplankton (e.g. > 20 mm). However, close to the surface, where densities of mesozooplankton were high (Fig. 9), this signal is likely to be influenced more strongly by the mesozooplankton, including *Calanus finmarchicus*. The upward shift in distribution of mesozooplankton observed with OPC, VPR and acoustics coincide with the shift towards more shallow depths of the larger copepods seen at the twilight MOCNESS station (Fig. 14), suggesting that these are among the taxa also responsible for the OPC and acoustic migration patterns observed.

For the echosounder bins where backscatter peaked at lower frequencies (e.g. 38 – 120 kHz), the distributions are either deep (e.g. > 300 m) or restricted to a few high density patches, and the support for DVM is limited (Fig. 7). The large-scale 38 kHz coverage presented in Norheim et al. (2016) and Klevjer et al. (submitted, this issue) shows that DVM of the mesopelagic scattering layers do not reach shallower than ~200 m in the Iceland Sea. During this time of year, vertical migration into the epipelagic is therefore likely dominated by organisms in the larger mesozooplankton and possibly smaller macrozooplankton size ranges.

In this study *Calanus* spp. makes up more than 50% of the food items by numbers, and the MOCNESS vertical distribution suggests that if *Calanus finmarchicus* migrates vertically, it does so predominantly within the upper 75–100 m of water (Fig. 14). This is in accordance with findings in Dale and Kaartvedt (2000). *Metridia* sp. occurs deep during day time (about 200 m) and makes more extensive vertical migrations to depths between 50 and 100 m at night (Fig. 14). Since euphausiids and amphipods also are known to migrate vertically (Kaartved, 2010; Havermans et al., 2019), all the prey taxa we observed in the herring stomachs are likely to be available to the herring in the upper 100 m, if herring also feed at night. If feeding is limited to daytime, the herring probably have to feed at depth to get abundant supplies of *Metridia* spp. and other species with DVM ranges of more than 100 m.

### 4.4. Herring migration, vertical distribution and environmental conditions

Broms et al. (2012) did not exclude the existence of a temperature limit for the herring, but suggested that such a limit would then appear to be different for herring at depth and in surface waters, since the herring reside at lower temperatures at depth. That study was based on a basin scale and seasonal data set. In the present study, herring were observed in water with temperatures from less than 1° to more than 5 °C, and from 300 to 0 m depths. In accordance with the observations by Broms et al. (2012), we found that the herring distributed towards lower temperatures in the west, and they also resided at lower temperatures at depth than at the surface in this area.

The physical front separating Atlantic and Arctic water masses also separated waters with low chlorophyll values on the Atlantic side from waters with higher chlorophyll values on the Arctic side (Figs. 2–4). As shown by the *in situ* light measurements (Fig. 15 A), the local productivity regime has strong implications for light conditions at depth. These variations in light levels again have large implications for the potential for visual predation (Fig. 15 B). The model predictions suggest that the resulting reduction in visual range is vertically structured; at 15 m the potential searched volume per day was reduced by less than 20% under the late-bloom conditions, whereas at 40 m depth the model predicts a ~90% reduction. The parametrization of the model we used in this run

was based on *Calanus finmarchicus* as a prey, for prey of different size and contrast the details of the results will differ, but a robust conclusion of the model results should be that the vertical extension of the herring niche is likely to be much larger pre-bloom. Post-bloom levels of chlorophyll in the Norwegian Sea remain at comparatively high levels (Rey, 2004; Erga et al., 2014, Naustvoll et al., this issue). As stated, the bloom in the Norwegian and Icelandic seas overall spread in a north-westerly direction, a herring that could "stay ahead" of the bloom in its migration would certainly be able to feed efficiently over a much larger depth range. Realized encounter rates would depend also on the available densities of prey, but density of prey is likely to increase in the surface water ahead of bloom initiation, as hibernating *Calanus finmarchicus* would need to ascend to the surface ahead of the bloom in order to match recruitment of its offspring's first feeding stage to the bloom peak (Melle et al., 2004).

At the time of our transect, we were in a post bloom environment in the Atlantic waters, while in Arctic waters we observed a late-bloom with a deep chlorophyll maximum (Fig. 2). As a consequence, optical conditions were likely more conducive to visual feeding east of the front, as chlorophyll levels there were the lowest (Figs. 2–4). The OPC data however suggested that the concentration of particle densities in the herring prey size range were very low in the upper waters during daytime (Fig. 6), and the herring stomachs from this area generally had little content (Fig. 13).

The vertical distribution of herring within and on both sides of the Arctic front as observed by hull-mounted acoustics, followed a known pattern (Misund et al., 1997; Nøttestad et al., 2007). On the Atlantic side, the herring were found in the upper 50 m during the day (Fig. 11). We did not have night-time observations there, but the herring tend to stay shallow both day and night in Atlantic water during summer (Misund et al., 1997). In the frontal area and in Arctic water west of the front, the herring were found both deep and shallow during daytime as well as at night (Fig. 11).

The deep distribution of herring near the Arctic front has been attributed to deep feeding at low temperatures, while returning to the surface waters with high temperatures to digest the food (Misund et al., 1997). Schools of herring were observed at depth in this area both day and night (Fig. 11). The prey types that were found in the stomachs of herring occurred over a range of depths in the MOCNESS catches, so the potential feeding habitat of herring occurred both in shallow and deeper waters (Fig. 14). Our data similarly show that once entering the Arctic water the herring change their vertical distribution from a constantly shallow distribution to both deep and shallow distributions. Across the front in the cold Arctic water, herring doubled their average stomach content, indicating that their behaviour results in increased feeding rates (Fig. 13), although reduced water temperatures may also slow down their digestion rate. In light of the results of the modelled visual ranges (Fig. 15), and given the higher chlorophyll levels found west of the Arctic front (Fig. 2), which in combination suggests poor visual conditions at depth in this area, we would have expected larger, more visible food items to be of higher importance to the herring here.

### 4.5. Predation and competition with macroplankton and micronekton

While some of the taxa caught in the Macroplankton trawl are important prey items for herring (e.g. amphipods, euphausiids), many of them may also be important as competitors.

Several of these taxa (e.g. euphausiids, amphipods, myctophids) occur with biomasses ranging from 1 to 5 g per $m^{-2}$. The average biomass of herring $m^{-2}$ sea surface was estimated at 1.85 g $m^{-2}$, which means that over the transect the herring biomass is ~1 order of magnitude lower than the sum of its competitors for *Calanus* as prey. These numbers suggest that the macroplankton and micronekton are important to the herring as both potential prey and competitors, and that the herring is only one of several competitors for *Calanus*. In early June, when the study was conducted, the nights are not particularly dark, but other taxa did show classical vertical migration patterns. During the time of the survey, scattering layers of mesopelagic fish migrated vertically, closely tracking light levels at depth, but the vertical migration was restricted, and the migrations did not reach the surface layers in the Iceland Sea, but terminated deeper than 200 m (Norheim et al., 2016). Since the mesopelagic fishes tend not to migrate all the way to the surface in Arctic water masses during the summer (Norheim et al., 2016), there may be less competition for prey in northerly areas during this time.

We did not register any predators of the herring, but we know there are killer whales, humpback, and minke whales, and birds like gannets that are abundant in the area. Schooling is the ultimate antipredator behaviour in the light summer months (Kaartvedt et al., 1998) and the vertical distribution of herring schools, seemingly not related to a typical DVM may be due to diving reactions related to the presence of predators or the ship.

## CRediT authorship contribution statement

**Webjørn Melle:** Conceptualization, Methodology, Writing - original draft, Writing - review & editing, Software. **Thor Klevjer:** Conceptualization, Methodology, Writing - original draft, Writing - review & editing, Software. **Espen Strand:** Conceptualization, Methodology, Writing - review & editing, Software. **Peter H. Wiebe:** Conceptualization, Methodology, Writing - review & editing, Software. **Aril Slotte:** Conceptualization, Methodology, Writing - review & editing, Software. **Geir Huse:** Conceptualization, Methodology, Writing - review & editing, Software.

## Declaration of competing interest

The authors declare that they have no known competing financial interests or personal relationships that could have appeared to influence the work reported in this paper.

## Acknowledgement

We would like to thank the captain and crew of R/V G. O. Sars for their skilled operations during our cruise from Bergen to Nuuk during May and June 2013. The sampling, data analysis and reporting have been supported by IMR through funding of shiptime, laboratory costs and salaries of researchers through internally funded projects. We would also like to acknowledge the funding from Euro-BASIN, EU FP7, Grant agreement No 264933, HARMES, Research Council of Norway project number 280546 and MEESO, EU H2020 research and innovation programme, Grant Agreement No 817669.

## References

Aksnes, D.L., Giske, J., 1993. A theoretical model of aquatic visual feeding. Ecol. Model. 67, 233–250.

Aksnes, D.L., Utne, A.C.W., 1997. A revised model of visual range in fish. Sarsia 82, 137–147.

Bachiller, E., Skaret, G., Nøttestad, L., Slotte, A., 2016. Feeding ecology of Northeast Atlantic Mackerel, Norwegian spring-spawning herring and blue whiting in the Norwegian sea. PLoS One 11 (2), e0149238. https://doi.org/10.1371/journal.pone.0149238.

Bagøien, E., Melle, W., Kaartvedt, S., 2012. Seasonal development of mixed layer depths, nutrients, chlorophyll and Calanus finmarchicus in the Norwegian Sea – a basin-scale habitat comparison. Prog. Oceanogr. 103, 58–79.

Basedow, S.L., Edvardsen, A., Tande, K.S., 2008. Vertical segregation of Calanus finmarchicus copepodites during the spring bloom. J. Mar. Syst. 70, 21–32.

Batty, R.S., Blaxter, J.H.S., Richard, J.M., 1990. Light-intensity and the feeding-behavior of herring, Clupea harengus. Mar. Biol. 107, 383–388.

Blaxter, J.H.S., 1964. Spectral sensitivity OF the herring, CLUPEA harengus L. J. Exp. Biol. 41, 155–162.

Blindheim, J., 2004. Oceanography and climate. In: Skjoldal, H.R. (Ed.), The Norwegian Sea Ecosystem. Tapir Academic Press, Trondheim, pp. 65–96.

Broms, C., Melle, W., 2007. Seasonal development of Calanus finmarchicus in relation to phytoplankton bloom dynamics in the Norwegian Sea. Deep Sea Res. (Part II, Topical Stud. Oceanogr.) 54 (23–26), 2760–2775.

Broms, C., Melle, W., Horne, J.K., 2012. Navigation mechanisms of herring during feeding migration: the role of ecological gradients on an oceanic scale. Mar. Biol. Res. 8, 461–474.
Broms, C., Melle, W., Kaartvedt, S., 2009. Oceanic distribution and life cycle of Calanus species in the Norwegian Sea and adjacent waters. Deep Sea Res. II 56, 1910–1921.
Brown, C.A., Huot, Y., Purcell, M.J., et al., 2004. Mapping coastal optical and biogeochemical variability using an autonomous underwater vehicle and a new bio-optical inversion algorithm: bio-optical inversion algorithms for AUVs. Limnol Oceanogr. Methods 2, 262–281.
Corten, A., 2002. The role of "conservatism" in herring migrations. Rev. Fish Biol. Fish. 11, 339–361.
Dale, T., Kaartvedt, S., 2000. Diel patterns in stage-specific vertical migration of Calanus finmarchicus in habitats with midnight sun. ICES J. Mar. Sci. 57 (6), 1800–1818.
Dalpadado, P., Ellertsen, B., Melle, W., Dommasnes, A., 2000. Food and feeding conditions of Norwegian spring-spawning herring (Clupea harengus) through its feeding migrations. ICES J. Mar. Sci. 57, 843–857.
Davis, C.S., Gallager, S.M., Berman, M.S., Haury, L.R., Strickler, J.R., 1992. The video plankton recorder (VPR): design and initial results. Archiv. fuer Hydrobiol., Beiheft: Ergeb. Limnol. 36, 67–81.
Davis, C.S., Hu, Q., Gallager, S.M., Tang, X., Ashjian, C.J., 2004. Real-time observation of taxa-specific plankton distributions: an optical sam-pling method. Mar. Ecol. Prog. Ser. 284, 77–96.
Demer, D.A., Berger, L., Bernasconi, M., Bethke, E., Boswell, K., Chu, D., Domokos, R., et al., 2015. Calibration of acoustic instruments, 326. ICES Cooperative Research Report, p. 130.
Dragesund, O., 1970. Distribution, abundance and mortality of young and adolescent Norwegian spring spawning herring(Clupea harengus Linne) in relation to subsequent year class strength. Fiskeridir. Skr. Ser. Havunders. 15, 451–556.
Dragesund, O., Johannessen, A., Ulltang, O., 1997. Variation in migration and abundance of Norwegian spring spawning herring (Clupea harengus L.). Sarsia 82, 97–105.
Drinkwater, K.F., Sundby, S., Wiebe, P.H., this issue. Exploring the hydrography of the boreal/arctic domains of North Atlantic seas: results from the 2013 BASIN survey.
Dupont, N., Bagoien, E., Melle, W., 2017. Inter-annual variability in spring abundance of adult Calanus finmarchicus from the overwintering population in the southeastern Norwegian Sea. Prog. Oceanogr. 152, 75–85.
Erga, S.R., Ssebiyonga, N., Hamre, B., Frette, O., Hovland, E., Hancke, K., Drinkwater, K., Rey, F., 2014. Environmental control of phytoplankton distribution and photosynthetic performance at the Jan Mayen Front in the Norwegian Sea. J. Mar. Syst. 130, 193–205.
Fernö, A., Pitcher, T., Melle, W., Nøttestad, L., Mackinson, S., Hollingworth, C., Misund, O.A., 1998. The challenge of the herring in the Norwegian Sea: making optimal collective spatial decisions. Sarsia 83, 149–167.
Foote, K., 1987. Fish target strengths for use in echo integrator surveys. J. Acoust. Soc. Am. 82, 981–987.
Gislason, A., Astthorsson, O.S., 2002. The food of Norwegian spring-spawning herring in the western Norwegian Sea in relation to the annual cycle of zooplankton. Sarsia 87 (3), 236–247.
Gislason, A., Logeman, K., Marteinsdottir, G., 2016. The cross-shore distribution of plankton and particles southwest of Iceland observed with a Video Plankton Recorder. Continent. Shelf Res. 123, 50–60.
Havermans, C., Auel, H., Hagen, W., Held, C., Ensor, N.S., Tarling, G.A., 2019. Predatory zooplankton on the move: Themisto amphipods in high-latitude marine pelagic food webs. In: Sheppard, C. (Ed.), Advances in Marine Biology, 82, p. 51.
Heino, M., Porteiro, F.M., Sutton, T.T., Falkenhaug, T., Godø, O.R., Piatkowski, U., 2011. Catchability of pelagic trawls for sampling deep living nekton in the mid-North Atlantic. ICES J. Mar. Sci. 68, 377–389. https://doi.org/10.1093/icesjms/fsq089.
Herman, A.W., 1992. Design and calibration OF a new optical plankton counter capable OF sizing small zooplankton. Deep-Sea Res. Part a-Oceanographic Research Papers 39, 395–415.
Holst, J.C., Dragesund, O., Hamre, J., Misund, O.A., Østvedt, O.J., 2002. Fifty years of herring migrations in the Norwegian Sea. ICES (Int. Counc. Explor. Sea) Mar. Sci. Symp. 215, 352–360.
Hu, Q., Davis, C.S., 2006. Accurate automatic quantification of taxa-specific plankton abundance using dual classification with correction. Mar. Ecol. Prog. Ser. 306, 51–61.
Huse, G., Fernö, A., Holst, J.C., 2010. Establishment of new wintering areas in herring co-occurs with peaks in the 'first time/repeat spawner' ratio. Mar. Ecol. Prog. Ser. 409, 189–198.
Huse, G., Holst, J.C., Utne, K., Nottestad, L., Melle, W., Slotte, A., Ottersen, G., et al., 2012. Effects of interactions between fish populations on ecosystem dynamics in the Norwegian Sea - results of the INFERNO project Preface. Mar. Biol. Res. 8, 415–419.
ICES, 2013. Report of the workshop on Northeast Atlantic Mackerel monitoring and methodologies including science and industry involvement (WKNAMMM), 25–28 February 2013, ICES headquarters, Copenhagen and hirtshals, Denmark, 18. ICES CM 2013/SSGESST, p. 33.
ICES, 1982. Report of the 1982 planning group on ICES-coordinated herring and sprat acoustic surveys. ICES Document CM 1982/H: 04.
ICES, 2008. Report of the Planning Group for Herring Surveys, vol. 1. ICES Document CM 2008/LRC, p. 256.
Jakobsson, J., Østvedt, O.J., 1999. A review of joint investigations on the distribution of herring in the Norwegian and Iceland Seas 1950-1970. Rit Fiskid. 16, 209–238.
Kaartved, S., 2010. Diel vertical migration behaviour of the Northern krill (Meganyctiphanes norvegica Sars). Adv. Mar. Biol. 57, 255–275.
Klevjer, T.A., Melle, W., Knutsen, T., Aksnes, D., submitted, this issue. Vertical Distribution and Migration of Mesopelagic Scatterers in Four North Atlantic Basins.
Kaartvedt, S., Knutsen, T., Holst, J.C., 1998. Schooling of the vertically migrating mesopelagic fish Maurolicus muelleri in light summer nights. Mar. Ecol. Prog. Ser. 170, 287–290.
Knutsen, T., Melle, W., Mjanger, M., Strand, E., Fuglestad, A.-L., Broms, C., Bagøien, E., Fitje, H., Ørjansen, O., Vedeler, T., 2013. Messor – a towed underwater vehicle for quantifying and describing the distribution of pelagic organisms and their physical environment. Proceedings of OCEANS13 MTS/IEEE konferanse i Bergen, June 2013, pp. 1–12. https://doi.org/10.1109/OCEANS-Bergen.2013.6608177.
Korneliussen, R.J., Heggelund, Y., Macaulay, G.J., Patel, D., Johnsen, E., Eliassen, I.K., 2016. Acoustic identification of marine species using a feature library. Methods Oceanogr. 17, 187–205. https://doi.org/10.1016/j.mio.2016.09.002.
Korneliussen, R.J., Ona, E., Eliassen, I., Heggelund, Y., Patel, R., Godø, O.R., et al., 2006. "The large scale survey system – LSSS,". Proceedings of the 29th Scandinavian Symposium on Physical Acoustics (Ustaoset).
Krafft, B.A., Melle, W., Knutsen, T., Bagøien, E., Broms, C., Ellertsen, B., et al., 2010. Distribution and demography of Antarctic krill in the southeast Atlantic sector of the southern ocean during the austral summer 2008. Polar Biol. 33, 957–968. https://doi.org/10.1007/s00300-010-0774-3.
Kvamme, C., Nøttestad, L., Fernö, A., Misund, O.A., Dommasnes, A., Axelsen, B.E., Dalpadado, P., Melle, W., 2003. Migration patterns in Norwegian spring-spawning herring: why young fish swim away from the wintering area in late summer. Mar. Ecol. Prog. Ser. 247, 197–210.
MacLennan, D.N., Fernandes, P.G., Dalen, J., 2002. A consistent approach to definitions and symbols in fisheries acoustics. ICES J. Mar. Sci. 59, 365–369. https://doi.org/10.1006/jmsc.2001.1158.
McQuinn, I.H., 1997. Metapopulations and the Atlantic herring. Rev. Fish Biol. Fish. 7, 297–329.
Melle, W., Abrahamsen, M., Valdemarsen, J.W., Ellertsen, B., Knutsen, T., 2006. Design and performance of a new macro-plankton trawl in combination with a multiple cod-end system. In SCOR Working Group 115, Mini Symposium on Standards for the Survey and Analysis of Plankton (Plymouth).
Melle, W., Ellertsen, B., Skjoldal, H.R., 2004. Zooplankton: the link to higher trophic levels. In: Skjoldal, Hein Rune (Ed.), The Norwegian Sea Ecosystem: 137-202. Tapir. Trondheim.
Melle, W., Runge, J., Head, E., Plourde, S., Castellani, C., Licandro, P., Pierson, J., Jonasdottir, S., Johnson, C., Broms, C., Debes, H., Falkenhaug, T., Gaard, E., Gislason, A., Heath, M., Niehoff, B., Nielsen, T.G., Pepin, P., Stenevik, E.K., Chust, G., 2014. The North Atlantic Ocean as habitat for Calanus finmarchicus: environmental factors and life history traits. Prog. Oceanogr. 129, 244–284. Part B.
Melle, W., Skjoldal, H.R., 1998. Reproduction and development of Calanus finmarchicus, C. glacialis and C. hyperboreus in the Barents sea. Mar. Ecol. Prog. Ser. 169, 211–228.
Misund, O.A., Melle, W., Fernö, A., 1997. Migration behaviour of Norwegian spring spawning herring when entering the cold front in the Norwegian Sea. Sarsia 82, 107–112.
Misund, O.A., Vilhjalmsson, H., Jakupsstovu, S.H.I., Røttingen, I., Belikov, S., Asthorsson, O., Blindheim, J., et al., 1998. Distribution, migration and abundance of Norwegian spring spawning herring in relation to the temperature and zooplankton biomass in the Norwegian Sea as recorded by coordinated surveys in spring and summer 1996. Sarsia 83, 117–127.
Morel, A., Claustre, H., Antoine, D., Gentili, B., 2007. Natural variability of bio-optical properties in Case 1 waters: attenuation and reflectance within the visible and near-UV spectral domains, as observed in South Pacific and Mediterranean waters. Biogeosci. Discuss. 4, 2417–2478.
Naustvoll, L., Melle, W., Klevjer T., Drinkwater, K., Strand, E., Knutsen, T., This Issue. Dynamics of Primary Production and Species Diversity of Phytoplankton in the North Atlantic during Spring and Summer - a Trans-Atlantic Survey.
Norheim, E., Klevjer, T.A., Aksnes, D.L., 2016. Evidence for light-controlled migration amplitude of a sound scattering layer in the Norwegian Sea. Mar. Ecol. Prog. Ser. 551, 45–52.
Nøttestad, L., Aksland, M., Beltestad, A., Fernö, A., Johannessen, A., Misund, O.A., 1996. Schooling dynamics of Norwegian spring spawning herring (Clupea harengus L.) in a coastal spawning area. Sarsia 80, 277–284.
Nøttestad, L., Misund, O.A., Melle, W., Ulvestad, B.K.H., Orvik, K.A., 2007. Herring at the Arctic front: influence of temperature and prey on their spatio-temporal distribution and migration. Mar. Ecol. 28, 123–133.
Olsen, E.M., Melle, W., Kaartvedt, S., Holst, J.C., Mork, K.A., 2007. Spatially structured interactions between a migratory pelagic predator, the Norwegian spring-spawning herring Clupea harengus L., and its zooplankton prey. J. Fish. Biol. 70, 799–815.
Rey, F., 2004. The phytoplankton. In: Skjoldal, Hein Rune (Ed.), The Norwegian Sea Ecosystem. Tapir, Trondheim, pp. 97–136.
Runnstrøm, S., 1941. Quantitative investigations on herring spawning and its yearly fluctuations at the west coast of Norway. Fiskeridir. Skr. Ser. Havunders. 6, 1–71.
Stenevik, E.K., Melle, W., Gaard, E., Gislason, A., Broms, C., Prokopchuk, I., Ellertsen, B., 2007. Egg production of Calanus finmarchicus-A basin-scale study. Deep Sea Res. (Part II, Topical Stud. Oceanogr.) 54 (23–26), 2672–2685.
Strand, E., Klevjer, T.A., Knutsen, T., Melle, W., This issue. Ecology of Mesozooplankton across Four North Atlantic Basins.
Utne, K.R., Huse, G., Ottersen, G., Holst, J.C., Zabavnikov, V., Jacobsen, J.A., Oskarsson, G.J., et al., 2012. Horizontal distribution and overlap of planktivorous fish stocks in the Norwegian Sea during summers 1995-2006. Mar. Biol. Res. 8, 420–441.
Varpe, Ø., Fiksen, Ø., 2010. Seasonal plankton–fish interactions: light regime, prey phenology, and herring foraging. Ecology 91, 311–318.

Voss, M., 1991. Content of copepod fecal pellets in relation to food-supply in Kiel-bight and its effect on sedimentation-rate. Mar. Ecol. Prog. Ser. 75 (2–3), 217–225.
Wenneck, T.D.L., Falkenhaug, T., Bergstad, O.A., 2008. Strategies, methods, and technologies adopted on the R.V. G.O. Sars MAR-ECO expedition to the Mid-Atlantic Ridge in 2004. Deep Sea Res. II 55, 6–28. https://doi.org/10.1016/j.dsr2.2007.09.017.
Wiebe, P.H., Morton, A.W., Bradley, A.M., Backus, R.H., Craddock, J.E., Cowles, T.J., Barber, V.A., Flierl, G.R., 1985. New developments in the MOCNESS, an apparatus for sampling zooplankton and micronekton. Mar. Biol. 87, 313–323.